The plasma membrane-associated cation-binding protein PCaP1 of Arabidopsis thaliana is a uranyl-binding protein

Alicia Vallet, Jacqueline Martin-Laffon, Adrien Favier, Benoît Revel, Titouan Bonnot, Claude Vidaud, Jean Armengaud, Jean-Charles Gaillard, Pascale Delangle, Fabienne Devime, et al.

The plasma membrane-associated cation-binding protein PCaP1 of *Arabidopsis thaliana* is a uranyl-binding protein

Alicia Vallet[a,1], Jacqueline Martin-Laffon[b,1], Adrien Favier[a,1], Benoît Revel[b], Titouan Bonnot[b,2], Claude Vidaud[c], Jean Armengaud[d], Jean-Charles Gaillard[d], Pascale Delangle[e], Fabienne Devime[b], Sylvie Figuet[b], Nelson B.C. Serre[b,3], Elisabetta Boeri Erba[a], Bernhard Brutscher[a], Stéphane Ravanel[b], Jacques Bourguignon[b,*] and Claude Alban[b,*]

[a]Univ. Grenoble Alpes, CEA, CNRS, IRIG, IBS, 38000 Grenoble, France

[b]Univ. Grenoble Alpes, CNRS, CEA, INRAE, IRIG, LPCV, 38000 Grenoble, France

[c]BIAM, CEA, CNRS, Univ. Aix-Marseille, 13108 Saint-Paul-lez-Durance, France

[d]Département Médicaments et Technologies pour la Santé (DMTS), Université Paris-Saclay, CEA, INRAE, SPI, F-F-30200 Bagnols-sur-Cèze, France

[e]Univ. Grenoble Alpes, CEA, CNRS, GRE-INP, IRIG, SyMMES, 38000 Grenoble, France

[1]These authors contributed equally to this work

[2]Present address: Agroécologie, INRAE, Institut Agro, Univ. Bourgogne, Univ. Bourgogne Franche-Comté, F-21000 Dijon, France

[3]Present address: Laboratoire de Reproduction et Développement des Plantes, Université de Lyon, UCB Lyon 1, ENS de Lyon, INRAE, CNRS, Lyon, France

*Corresponding authors:

claude.alban@cea.fr; +33 438 78 33 83

Univ. Grenoble Alpes, INRAE, CEA, CNRS, IRIG, LPCV, 38000 Grenoble, France

jacques.bourguignon@cea.fr; +33 438 78 46 88

Univ. Grenoble Alpes, CEA, INRAE, CNRS, IRIG, LPCV, 38000 Grenoble, France

Keywords: plant, uranium, radionuclide, metal, binding, fluorescence spectroscopy, solution state NMR, translocation

Highlights

- Metalloproteomics analysis identified 38 UraBPs from Arabidopsis roots and/or shoots.
- Recombinant PCaP1 protein (UraBP25) binds up to 2 U(VI) ions with high affinity *in vitro*.
- Recombinant PCaP1 protein binds about 15 Cu(II) or 60 Fe(III) ions *in vitro*.
- U(VI) binding triggers PCaP1 oligomerization.
- U(VI) translocation capacity is reduced in an Arabidopsis *pcap1-null* mutant.

Abstract

Uranium (U) is a naturally-occurring radionuclide that is toxic to living organisms. Given that proteins are primary targets of U(VI), their identification is an essential step towards understanding the mechanisms of radionuclide toxicity, and possibly detoxification. Here, we developed an immobilized metal affinity chromatography procedure to trap protein targets of uranyl from *Arabidopsis thaliana*. This procedure allowed the identification of 38 uranyl-binding proteins (UraBPs) from root and shoot extracts. One of these, UraBP25, previously identified as plasma membrane-associated cation-binding protein 1 (PCaP1), was further characterized for its ability to interact with U(VI) and other metals *in vitro*, by spectroscopic and structural approaches, and *in planta*, by analyzing the fate of U(VI) in Arabidopsis lines affected in *PCaP1* gene expression. Our results showed that recombinant PCaP1 binds U(VI) *in vitro* with affinity in the nM range, as well as Cu(II) and Fe(III) in high proportions, and that Ca(II) competes with U(VI) for binding. U(VI) induced PCaP1 oligomerization through binding at the interface of monomers, both at the N-terminal structured domain and the C-terminal flexible region. Finally, U(VI) translocation in Arabidopsis shoots was affected in a *pcap1* null-mutant, suggesting a role for this protein in ions trafficking *in planta*.

1. Introduction

Uranium (U) is a radionuclide naturally present in the Earth's crust. It is mainly redistributed in the environment by human activities (e.g. industry, agriculture, mining) and can accumulate locally to concentrations that present potential risks for ecosystems, agrosystems, and eventually human health. Indeed, this element is chemotoxic and possibly radiotoxic for all living organisms. In most natural settings, the di-oxo uranyl cation UO_2^{2+} is the most stable form of U, with U in the +VI oxidation state (thereafter referred to as U(VI)). Although U(VI) is not essential for plants, it is absorbed from the soil, incorporated into the biomass, and thus enters the food chain. Consequently, contamination of soils by U(VI) and its absorption by plants represent a substantial health risk for humans. As predicted by the hard and soft acids principle, uranyl cation is a hard acid and has a high propensity to interact with hard oxygen donors, primarily by electrostatic bonding (Pearson, 1963). Therefore, the biological ligands of U(VI) may be as wide as metabolites, nucleic acids and polypeptides (Garai and Delangle, 2020). Since uranyl has the ability to bind strongly to biomolecules through carboxylate and phosphate groups (two of the main hard oxygen donors), proteins may be considered as primary targets of U(VI). Thus, identifying protein targets of uranyl is a crucial step in an attempt to decipher the molecular bases of radionuclide toxicity, and perhaps their detoxification, in any living being (Sarthou et al., 2020).

In the last decade, various strategies have been developed for the identification of proteins with high-affinity and/or selectivity for uranyl and forming uranyl-protein complexes *in vivo* and/or *in vitro* (Acharya and Blindauer, 2016; Basset et al., 2013; Bucher et al., 2014; Creff et al., 2019; Eb-Levadoux et al., 2017; Gallois et al., 2021; Huynh et al., 2015; Pardoux et al., 2012; Qi et al., 2014; Safi et al., 2013; Vidaud et al., 2019; Xu et al., 2014). Most of them were metalloproteomic approaches combining efficient protein separation techniques with powerful and sensitive protein and metal identification devices, namely protein tandem mass spectrometry (MS/MS) and inductively coupled plasma mass spectrometry (ICP-MS), respectively. These investigations identified a wide range of proteins that bind uranyl in various organisms including archaea, bacteria, animals and humans. Their discovery was an important milestone for understanding the cellular toxicity of the radionuclide (Basset et al., 2013; Cvetkovic et al., 2010; Dedieu et al., 2009; Gallois et al., 2021; Huynh et al., 2016; Xu et al., 2014). Uranyl-binding proteins (UraBPs) are implied in calcium homeostasis (for example calmodulin, fetuin-A and osteopontin), iron homeostasis (ferritin and transferrin), glucose metabolism, oxidative stress response, microtubule and actin cytoskeleton regulation, or proteolysis. Despite the large number of studies published to date on the impact of U(VI) exposure on plant physiology and development, and on its fate upon absorption (Aranjuelo et al., 2014; Berthet et al., 2018; Doustaly et al., 2014; Ebbs et al., 1998; Lai et al., 2020; Laurette et al., 2012; Misson et al., 2009; Saenen et al., 2014; Saenen et al., 2015; Sarthou et al., 2020;

Serre et al., 2019; Tewari et al., 2015; Vanhoudt et al., 2014), no plant UraBP has been identified so far. Yet, such discoveries can help to better understand the molecular mechanisms that govern the fate of U(VI), and understanding how plants manage to thrive in contaminated environmental ecosystems. This knowledge is also required for a future sustainable management of U(VI) in polluted soils and waters as well as in the food chain (Berthet et al., 2018).

In this study, we developed a successful two-stage enrichment procedure (ion-exchange chromatography prefractionation step followed by affinity capture) to identify protein targets of uranyl in *Arabidopsis thaliana*. This procedure enabled the purification of 38 UraBP from root and/or shoot extracts by shotgun proteomics. One of these proteins, named UraBP25 (25th U(VI)-interacting protein of our list), hitherto-identified as the plasma membrane-associated cation-binding protein 1 (PCaP1), was of particular interest. PCaP1 was further characterized for its ability to interact with U(VI) and other metals *in vitro*, by a combination of biochemical and structural approaches, and *in planta*, by analyzing the fate of U(VI) in Arabidopsis lines affected in the expression of the corresponding gene. Taken together, our results showed first, that recombinant PCaP1 binds U(VI) *in vitro* with high affinity and Cu(II) and Fe(III) in high proportions, and that Ca(II) competes with U(VI) for binding. Second, we showed that U(VI) induces PCaP1 oligomerization through binding to both the N-terminal structured protein domain and the C-terminal flexible region. Last, we observed that U(VI) translocation in Arabidopsis shoots is affected in a *pcap1* null-mutant suggesting a role *in planta* for this protein in cations mobility.

2. Materials and Methods

2.1. Plant growth conditions for protein fractionation studies

Sterilized and stratified seeds of wild-type *Arabidopsis thaliana* ecotype Columbia (Col-0) were sown into homemade thermoprinted plates, as described previously (Sarthou et al., 2022). Plants were grown in hydropony for 5 weeks in the 'Gre medium' nutrient solution, as detailed in (Sarthou et al., 2022), with weekly solution changes. Growth was performed in a controlled environment, with alternation of 8 h light period at 22°C (light intensity of 110 µmol of photons $m^{-2}s^{-1}$) and 16 h dark period at 20°C.

2.2. Preparation of protein extracts and anion exchange chromatography (AEC) fractionation

Total soluble proteins from plant shoot and root tissues were extracted by grinding 15 g powdered samples in 10 mM Tris-HCl, pH 7.5, 1 mM dithiothreitol, and a cocktail of protease inhibitors (Roche Applied Science). Samples were clarified by centrifugation, desalted on PD10 Sephadex G25 (M) columns (GE Healthcare), and 30-40 mg soluble proteins were then

fractionated by chromatography onto Q-Sepharose High Performance columns (1.6 x 5 cm), as described previously (Sarthou et al., 2020). Stepwise elution was performed using discontinuous increasing NaCl concentrations in the extraction buffer (from 0 to 1 M NaCl; Sub-fractions F0 to F1000). The salt concentrations were chosen to obtain a homogenous repartition of the quantity of proteins in each sub-fraction (Supplementary Figure S1). Collected sub-fractions were stored at -80°C until used for further analyses. Four independent fractionation experiments from independent 8-plant cultures each were performed (Series 1 to 4).

2.3. Protein determination

Proteins from plant extracts were measured by the Bradford method using Bio-Rad protein assay reagent, with bovine serum albumin as a standard (Bradford, 1976). Protein AEC sub-fraction aliquots (30 µg) were analyzed by SDS-PAGE 12% and staining with Coomassie Brilliant Blue R250, as described (Sarthou et al., 2020).

2.4. Protein capture by immobilized metal affinity chromatography (IMAC)

Anion exchange chromatography (AEC) eluted proteins from leaf and root extracts were divided in a rational way into 2 and 3 main homogenous fractions, respectively, covering the whole polypeptide profiles (herein named leaf LA3, LB3 and LA4, LB4 fractions and root RA3, RB3, RC3 and RA4, RB4 and RC4 fractions, from Series 3 and 4, respectively). Protein fraction aliquots were then adjusted to 0.05 to 0.1 mg/mL with binding buffer (50 mM Hepes, pH 7.4, 0.5 M NaCl, 0.05% (w/v) Brij) and extensively dialyzed overnight against the binding buffer. High salt concentration and surfactant supplementation in the binding buffer aimed at minimizing non-specific interactions with the IMAC matrix (Dedieu et al., 2009). After addition of 5 µL/mL of 0.2 M $NaHCO_3$ (a chelating agent for uranyl cations which acts as a competitor for proteins with low uranyl affinity, when used at low concentration), to prevent weak interactions, 1-2.5 mL fraction aliquots were put in contact with 50 µL freshly prepared and conditioned U(VI)-loaded and U(VI)-free (chromatographic blanks) Duolite C467 beads (Basset et al., 2008; Dedieu et al., 2009), and stirred gently for 1 h at room temperature. The supernatants (flow through) were put aside after centrifugation and the beads washed extensively with binding buffer and dialyzed overnight at 4°C to remove any non-specifically bound proteins. Then, the proteins were eluted with 600 µL of 0.2 M $NaHCO_3$, for 90 min (Vidaud et al., 2019). The eluates were collected, concentrated to a final volume of 60 to 200 µL using a micro-concentrator system (Amicon® Ultra, Ultracel® - 3K, 3-kDa cutoff; Millipore) and stored at -20°C until use for further protein identification. Flow through fractions were concentrated and stored in the same way.

2.5. Identification of the captured proteins by high-resolution tandem mass spectrometry

Ten µL aliquots of proteins (concentrated flow through or eluted fractions) were supplemented with 20 µL of 1.5X Laemmli LDS buffer (Invitrogen). Samples were heated for 5 min at 99°C,

centrifuged for 1 min, and the resulting supernatants loaded onto a NuPAGE 4-12% Bis-Tris gel (Invitrogen). After a short denaturating electrophoresis of 4 min at 200 V, gel bands containing the LDS-soluble proteomes were excised and processed for an in-gel trypsin proteolysis, as previously described (Hartmann et al., 2014). The resulting peptides were analyzed using a LTQ Orbitrap XL mass spectrometer (Thermo Fischer Scientific) coupled to an Ultimate 3000 nanoRSLC nano LC system (Dionex-LC Packings). A volume of 10 µL (out of 50 µL) of peptides was injected and desalted on-line on a reverse-phase Acclaim PepMap100 C18 micro precolumn (5 µm bead size, 100 Å pore size, 300 µm internal diameter, 5 mm length, Thermo Fisher Scientific) and then separated on an Acclaim PepMap100 C18 nano column (3 µm bead size, 100 Å pore size, 75 µm internal diameter, 15 cm length, Thermo Fisher Scientific) at a 0.2 µL/min flow rate with a 4-48% gradient of solvent B (99.9% CH_3CN, 0.1% HCOOH) against solvent A (99.9% H_20, 0.1% HCOOH). Each run was preceded by at least one blank run avoid cross-contamination. Data-dependent acquisition was done on peptides with potential charges of either 2+ or 3+. Full-scan mass spectra were recorded at a resolution of 30,000 from 300 to 1800 *m/z* with an automatic gain control target set at 5 x 10^5 ions. MS/MS scans were acquired on the three most abundant ions, selecting ions with a dynamic exclusion of 60 s of all previously fragmented peptide ions. MS/MS spectra were assigned to peptide sequences (p value ≤ 0.05) using the MASCOT search engine (version 2.5.1, Matrix Science) against the protein sequences of the SwissProt database (SwissProt 2015_02 download), selecting *Arabidopsis thaliana* as organism (13,640 protein sequences). MS and MS/MS mass tolerances were set to 5 ppm and 0.5 Da, respectively. The other search parameters were: a maximum of two trypsin miss-cleavages, systematic carbamidomethylation of cysteine, as well as deamidation of glutamine and asparagine and oxidation of methionine as three possible dynamic modifications. Proteins were identified when at least two different peptide sequences were assigned. The abundance of the identified proteins in each fraction was assessed by their spectral counts (number of MS/MS spectra assigned per protein).

2.6. Proteomics data deposition

The proteomics data have been deposited to the ProteomeXchange Consortium via the PRIDE (Perez-Riverol et al., 2019) partner repository with the dataset identifier PXD033354 and 10.6019/PXD033354. [The dataset is available with the Username: reviewer_pxd033354@ebi.ac.uk and Password: 62dQFqjg].

2.7. Cloning of PCaP1 cDNA forms for recombinant proteins production

Sequences of primers used in this study are listed in Supplementary Table S1. Full-length *PCaP1* (At4g20260) and splicing variant *PCaP1v* cDNA coding sequences were amplified by RT-PCR using total RNA isolated from 3-week-old Arabidopsis leaves with the RNeasy plant mini extraction kit (Qiagen) and reverse-transcribed with the ThermoScript RT-PCR system

(Invitrogen). The cDNA fragments were amplified by PCR with primers introducing *Nco*I and *Sal*I restriction sites upstream the initiation codon and downstream the stop codon, respectively (Supplementary Table S1). The PCR products were sequenced (Eurofins) and ligated into the pET28b+ plasmid (Novagen) between the *Nco*I and the *Sal*I sites to obtain the pET28-PCaP1 and pET28-PCaP1v recombinant plasmids, respectively. The cDNA encoding the truncated PCaP1 form, PCaP1Δ, was obtained by PCR amplification using pET28-PCaP1 plasmid as a matrix and specific primers (Supplementary Table S1). The PCR product was ligated into the pET28b+ plasmid to obtain the pET28-PCaP1Δ recombinant plasmid. The resulting pET28-PCaP1 constructs were amplified into *Escherichia coli* DH5α cells and then introduced into the *E. coli* overexpression host Rosetta 2 (DE3) (Stratagene).

2.8. Production and purification of the recombinant PCaP1 forms

The transformed cell cultures were grown at 37°C in lysogeny broth (LB) medium supplemented with the appropriate antibiotics until A_{600} was 0.6. Then, isopropylthioβ-D-galactoside was added to a final concentration of 0.4 mM and incubations pursued for 15 h at 37°C. Cell pellets from 2-L cultures were resuspended in 50 mL of extraction buffer containing 20 mM Tris-HCl, pH 8, 10% (w/v) glycerol, 1 mM dithiothreitol and a cocktail of complete protease inhibitors (Roche Applied Science), and then disrupted by sonication with a Vibra-Cell disrupter (Branson Ultrasonics). Cell debris were eliminated by centrifugation at 40,000 x g for 30 min and soluble proteins recovered from supernatants were subjected to ammonium sulphate precipitation at 4°C with crystalline ammonium sulphate to 50% saturation. The resulting precipitates were collected by centrifugation (40,000 x g, 15 min, 4 °C), resuspended in 10 mM potassium phosphate buffer, pH 7 supplemented with protease inhibitors and dialyzed overnight at 4°C against 4 L of 10 mM phosphate buffer, pH 7. Protein samples were applied onto a Bio-Gel HTP hydroxylapatite column (2.6 x 7 cm, Bio-Rad) equilibrated with 10 mM potassium phosphate buffer pH 7. Proteins were eluted with a linear gradient of phosphate buffer from 10 to 350 mM potassium phosphate (320 mL) at a flow rate of 0.5 mL/min. Five-mL fractions were collected. Fractions containing recombinant PCaP1 proteins were pooled and desalted by successive concentrations/dilutions with 10 mM Tris-HCl buffer, pH 7.5 containing 10% (w/v) glycerol, using Amicon® Ultra-15 centrifugal filtration units (3 kDa cut-off; Millipore). Samples were then loaded onto a Fractogel EMD-DEAE (650 M) column (1.6 x 5 cm; Merck) equilibrated with 10 mM Tris-HCl, pH 7.5 buffer containing 10% (w/v) glycerol. After extensive wash of the column with five volumes of buffer, proteins were eluted using a 150-mL linear gradient from 0 to 500 mM NaCl in this buffer, at a flow rate of 0.5 mL/min. PCaP1-containing fractions were pooled and concentrated before being applied onto a Hiload® Superdex 75 column (1.6 X 60 cm, Cytiva) equilibrated with 10 mM Tris-HCl buffer, pH 7.5 containing 10% (w/v) glycerol and 150 mM NaCl. Elution was conducted in the same

buffer at a flow rate of 1 mL/min. Purified recombinant proteins were finally concentrated and stored aliquoted at -80°C, until used. Protein purity and integrity were monitored by SDS-PAGE and mass spectrometry under denaturing conditions. Purified protein concentration was determined by recording UV absorption spectra, using a NanoDrop 2000 spectrophotometer (Thermo Fischer Scientific) (Mass Extinction Coefficients at 280 nm were $E_{1\%}$ = 4.66 Lg^{-1} cm^{-1} for PCaP1; 5.70 for PCaP1v and 7.32 for PCaP1Δ, as calculated from the Molar Extinction Coefficient ε_{280} = 11460 M^{-1} cm^{-1}, ProtParam ExPASy).

Production and purification of recombinant PCaP1 protein uniformly labelled with ^{15}N and ^{13}C (*U*-^{15}N,^{13}C-PCaP1) or labelled with ^{15}N and ^{2}H (^{2}H,^{15}N,-PCaP1) was performed similarly as for unlabeled protein, except that growth was conducted in 2 L of a minimal M9 medium, containing antibiotics and supplemented with either ^{15}N-NH_4Cl (15N, 99%) and ^{13}C-glucose (U-13C6, 99%) or ^{15}N-NH_4Cl (15N, 99%) and D_2O (99.9%) (Cambridge Isotope Laboratories, Inc.), respectively, after progressive medium acclimatization from pre-cultures conducted in LB medium.

The presence of recombinant PCaP1 in eluted fractions during the purification process was assessed by western-blotting, initially using a commercially available polyclonal rabbit antibody raised against KLH-conjugated peptide derived from the Arabidopsis PCaP1 sequence (1:2000 dilution) (Agrisera; Ide et al. (2007)), and subsequently using a more sensitive custom-made rabbit polyclonal PCaP1 antibody raised against the whole purified recombinant protein (1:50000 dilution) (Covalab). Proteins were separated by SDS–PAGE, electro-transfered to nitrocellulose membrane and probed using the PCaP1 antibody and horseradish peroxidase-conjugated anti-rabbit IgGs (Bio-Rad). Protein detection was achieved using the ECL Plus™ Western Blotting detection reagents and a Typhoon 9400 imager (Cytiva).

2.9. Native mass spectrometry

Mass Spectrometry under native conditions was performed to determine the oligomeric state of PCaP1. Prior to analysis, purified protein (a 100-µL 50 µM aliquot) was extemporaneously chromatographed onto a Superdex 200 Increase 10_300 GL column equilibrated with 250 mM ammonium acetate, pH 8, for buffer exchange. Protein was injected in the spectrometer at a 7 µM final concentration. A nanoflow electrospray (nano-ESI) source and Nanoflow platinum-coated borosilicate electrospray capillaries (Thermo Electron SAS, Courtaboeuf, France) were used to generate ions (Boeri Erba et al., 2018; Puglisi et al., 2020). A quadrupole time-of-flight mass spectrometer (Q-TOF Ultima, Waters Corporation, Manchester, U.K.) modified for the detection of high masses was operated with the following parameters: capillary voltage = 1.2–1.3 kV, cone potential = 40 V, RF lens-1 potential = 40 V, RF lens-2 potential = 1 V, aperture-1 potential = 0 V, collision energy = 30–140 V, and microchannel plate (MCP) = 1900 V. The mass spectrometer was calibrated externally with a solution of cesium iodide at 6 mg/mL dissolved in 50% isopropanol. Mass spectra were processed using the Masslynx 4.0 software

(Waters Corporation, Manchester, U.K.), Massign software package (Morgner and Robinson, 2012) and UniDec (Marty et al., 2015).

2.10. Metal-binding affinities measured by fluorescence titration

Fluorescence spectroscopy was performed using a MOS450 Bio-Logic spectro-fluorimeter (Bio-Logic-Science Instruments, Claix, France) set at 277 nm for excitation. The slit widths for emission and excitation were set at 8 nm. The spectro-fluorimeter was driven by Bio-Kine 32 4.1 software. The measurements were performed at 25°C, in a 1 cm path cell.

For fluorescence titrations of PCaP1 in the presence of copper ($CuCl_2$), ferric iron ($Fe(NO_3)_3$) or calcium ($CaCl_2$), we used a 0.8 µM protein solution in 10 mM Tris-HCl pH 7.5 or 10 mM MES pH 6 buffer with 100 mM NaCl. The fluorescence was transmitted through a long pass filter (FF01-300/LP-25, Semrock) and emission was collected at 342-348 nm. The apparent dissociation constant ($K_d$app) and the stoichiometry of metal binding to PCaP1 (*n*) were determined using the fluorescence titration curves. The variation of PCaP1 fluorescence intensity as a function of the metal concentration was analyzed by using the following equation (Eq. 1) as described (Nagasaki-Takeuchi et al., 2008):

(1)

$$(F_0 - F) = \frac{\Delta Fmax \times [Metal]}{K_d app + [Metal]}$$

where, F_0 and F are fluorescence intensities measured at 342-348 nm without or with the presence of metal, respectively; ΔF_{max} is the maximum fluorescence change observed when the protein is fully saturated at the specific metal-binding sites with an apparent affinity of $K_d$app in a binding-site dependent manner; [Metal] and [PCaP1] are concentrations of free metal and PCaP1 in the assay, respectively. We also applied the following equation (Eq. 2) to determine the ligand-binding number (*n*) with the postulate that PCaP1 has *n* binding sites with identical affinity (Nagasaki-Takeuchi et al., 2008):

(2)

$$\frac{1}{F_0 - F} = \frac{2n}{\Delta Fmax} \times \frac{1}{[Metal]/[PCaP1]} + \frac{1}{\Delta Fmax}$$

Fitting of the data was performed with KaleidaGraph 4.51 software (Synergy Software, PA, USA).

For fluorescence titrations of PCaP1 in the presence of U(VI), we used a 0.8 µM protein solution in 10 mM MES pH 6 buffer with 100 mM NaCl. Iminodiacetate (IDA) was added to the protein solutions at a IDA:protein ratio of 12.5:1 to prevent the appearance of hydroxo complexes and to control U(VI) speciation (Pardoux et al., 2012). Fluorescence emission spectra were acquired from 280 to 470 nm. Competition experiments between the PCaP1 proteins and IDA were performed to calculate the conditional stability constants of the U(VI)-

protein complexes at pH 6. IDA binds uranyl with mild affinity and forms the UO_2IDA, $[UO_2(IDA)_2]^{2-}$ and $[(UO_2)_2(IDA)_2(OH)_2]^{2-}$ complexes. The conditional stability constants of these three species at 25°C and 0.1 M ionic strength were calculated from published global constants (Jiang et al., 2002; Starck et al., 2015). These values were set up in the spectral data analyses, which were performed using the SPECFIT software (Binstead et al., 2003; Gampp et al., 1985). Several models for the UO_2^{2+}-protein complexes were assayed, and only the one predicting a $UO_2(Protein)_2$ specie only gave a good fit for the experimental data. The model considering a non-luminescent complex was the most reliable. Experiments were repeated to ensure reproducibility.

2.11. Metal quantification in metal-protein complexes by Size Exclusion Chromatography (SEC) and Inductively Coupled Plasma-Mass Spectrometry (ICP-MS)

Metal-protein complexes were prepared by incubating 10 µM purified PCaP1 solutions for 15 min at 25°C, in 20 mM Tris-HCl pH 7.5, or 20 mM MES pH 6 buffer containing 150 mM NaCl and 2 mM $CuCl_2$, 2 mM $Fe(NO_3)_3$, 10 mM CaC_2 or 50 µM $UO_2(NO_3)_2$, as indicated. Formed complexes were separated from unbound metals by SEC, through centrifugation for 2 min at 724g of the samples (150 µL), on MicroSpin™ G-25 columns (Cytiva), equilibrated with the appropriate working buffer (Tris-HCl/NaCl or MES/NaCl). Controls without protein were run in parallel for background correction. Binding assays were performed at least in triplicate for each metal. Protein in the eluates was quantified by recording A_{280}. Eluates (50 µL aliquots) were then incubated with 10% (v/v) HNO_3 (Suprapur, Merck) for 2h at 60°C to ensure protein denaturation and release of bound elements. Precipitated proteins were removed by centrifugation and the mineralized samples were then diluted in 0.5% (v/v) HNO_3 and analyzed by ICP-MS using an iCAP RQ quadrupole mass instrument (Thermo Fisher Scientific GmbH, Germany), as detailed previously (Sarthou et al., 2020). Elements (^{44}Ca, ^{56}Fe, ^{57}Fe, ^{63}Cu, ^{65}Cu, ^{238}U) were analyzed using the standard mode and the collision mode with helium as a cell gas. Elements concentration was determined using standard curves and corrected using a solution of ^{45}Sc, ^{103}Rh and ^{172}Yb, as an internal standard. Data integration was performed using the Qtegra software (Thermo Fisher Scientific GmbH, Germany).

2.12. Solution-state Nuclear Magnetic Resonance (NMR) studies

NMR experiments were performed on Bruker Avance IIIHD spectrometers operating at magnetic field strengths of 16.5, 20, and 22.3 T (^1H Larmor frequency of 700, 850 and 950 MHz). All spectrometers were equipped with helium-cooled triple-resonance probes (HCN TCI 5mm) and pulsed z-field gradients. NMR assignments were obtained from a set of 3D Band-selective Excitation Short-Transient Transverse Relaxation-Optimized Spectroscopy (BEST-TROSY) (Favier and Brutscher, 2011) type correlation experiments: HNCO, HNCACO, HNCA, HNCOCA, HNCACB, and HNCOCACB. These experiments were performed on uniformly

$^{13}C/^{15}N$ labeled PCaP1 samples (in 10 mM Tris-HCl, pH 7.5 buffer, at 300K) and sample concentrations ranging from 100 to 500 μM.

Translational diffusion constants of the proteins in solution were measured by 1D ^{1}H Diffusion Ordered Spectroscopy (DOSY) experiments (Johnson, 1999) focusing either on the methyl or amide spectral region. A series of 1D spectra was recorded with varying gradient strength and a total acquisition time of about 15 min.

^{15}N relaxation experiments (T_1 and T_2) were performed on uniformly ^{15}N-labeled full-length PCaP1 on the free form and in complex with U(VI) using standard NMR pulse sequences (Farrow et al., 1994). The ^{15}N T_1 signal decay was sampled for 12 time points varying between 0 to 1.8 s while ^{15}N T_2 relaxation experiments were recorded with relaxation delays ranging from 0 to 280 ms.

NMR titration experiments were performed by adding up to 5-fold excess of U(VI) to either full-length PCaP1 or PCaP1Δ and recording at each titration step a 2D ^{1}H-^{15}N BEST-TROSY spectrum.

All NMR experiments handled in this study were implemented in the NMRlib pulse sequence library (Favier and Brutscher, 2019) that can be freely downloaded from the IBS website (*http://www.ibs.fr/research/scientific-output/software/pulse-sequence-tools*). The experiments were processed and analyzed using Bruker Topspin 3.5 and CCPNMR V3 software (Collaborative Computing Project for NMR; https://ccpn.ac.uk/software/downloads/).

2.13. Characterization, genetic complementation and U(VI) treatment of the Arabidopsis pcap1.4 mutant

Seeds of the Arabidopsis *pcap1.4* knockout mutant (Li et al., 2011; Nagata et al., 2016) were obtained from the Arabidopsis Biological Resource Center (registration no. SAIL_241_A08). Homozygous status of the T-DNA insertion line was checked by PCR, using gene-specific and T-DNA border primers (Supplementary Table S1). The T-DNA insertion sites within exon 4 of *PCaP1* gene (Li et al., 2011) were confirmed by sequencing. For genetic complementation experiments, the complete coding sequence of *PCaP1* was fused to a double enhanced 35S promoter using the plasmid pFP101 containing a green fluorescent protein (*GFP*) reporter gene (Bensmihen et al., 2004). This construct was introduced into homozygous *pcap1.4* plants by the Agrobacterium-mediated floral-dip transformation method (Clough and Bent, 1998). Transformed seeds expressing the GFP marker were selected by fluorescence detection. All primer sequences are available in Supplementary Table S1. PCaP1 expression in Arabidopsis lines was checked by western blot analysis of total proteins extracted from leaves with 10 mM Tris-HCl, pH 7.5 buffer, containing 1 mM dithiothreitol, 1% SDS and a cocktail of protease inhibitors (Roche Applied Science), using custom-made PCaP1 antibody.

For U(VI) treatment, plants were first grown in hydropony for 5 weeks in Gre medium with weekly solution changes until treatment, and transferred to Gre medium depleted with

phosphate and complemented with 20 µM uranyl nitrate ($UO_2(NO_3)_2$). Plants were harvested 1 to 11 days after U(VI) treatment. To remove U(VI) weakly bound on the root surface, the plants were first rinsed once with 10 mM Na_2CO_3, then twice with distilled water. Photosystem II efficiency in dark-adapted leaves (Fv/Fm) was assessed using a FluorPen (FP100/D, Photon Systems Instruments, Brno, Czech Republic) and used as an indicator of plant health. Roots and shoots were separated, quickly dried on absorbing paper and fresh biomass was then determined. Finally, roots and shoots were dehydrated at 80°C for 24 h and dried samples were mineralized in 0.5-1 ml of 65% (w/v) HNO_3 (Suprapur, Merck), diluted in distilled water and analyzed by ICP-MS, as described previously (Sarthou et al., 2022).

Statistical analyses were performed using the R Studio software (RStudio Team, 2015) and the *nparcomp* package (Konietschke et al., 2015). Statistical significance was determined using non-parametric Tukey tests conducted with a confidence level set at 99% ($p < 0.01$).

3. Results

3.1. *Identification of 38 UraBPs from Arabidopsis roots and shoots captured by IMAC on U(VI)-loaded beads*

To isolate UraBPs from plant extracts, we used the efficient uranyl-loaded Duolite C467™ matrix previously developed for the identification of UraBPs from human serum, kidney-2 and dopaminergic SH-SY5Y cells (Basset et al., 2008; Dedieu et al., 2009; Vidaud et al., 2019). The experimental design is depicted in Figure 1. Soluble proteomes isolated from roots and leaves from hydroponically grown *Arabidopsis thaliana* plants were first pre-fractionated by anion exchange chromatography (AEC) on High Performance Q-Sepharose column. Protein concentration profiles and SDS-PAGE analysis of the sub-fractions obtained from four independent biological experiments are presented in Supplementary Figure S1. This fractionation procedure reduced the complexity of the protein samples in a very reproducible way and enriched the less abundant proteins facilitating their capture and identification. As an example, in the case of the leaf proteome, the method allowed to separate the very abundant Rubisco protein (present in the LB fraction) from less abundant proteins displayed in the LA fraction (Supplementary Figure S1). In the case of the root proteome, the method led to the separation of three enriched homogenous protein fractions, RA, RB and RC.

Two of the four-fractionation experiments conducted with Arabidopsis root and shoot tissues (Series 3 and 4, Supplementary Figure S1) were used as starting biological materials (biological duplicate, experiments 1 and 2) to capture UraBPs by immobilized metal affinity chromatography (IMAC) on U(VI)-loaded beads in a batch system, and to subsequently identify them by mass spectrometry (Figure 1). Fractionation experiments from series 1 and 2 were set aside for analyses unrelated to this work (unpublished data). All the specifically captured proteins obtained from the ten IMAC experiments (five from experiment 1 and five from

experiment 2), as well as the corresponding flow through supernatants were submitted to nanoLC-ESI MS/MS analysis for identification (Supplementary Table S2). The IMAC process including the capture conditions and the washing steps was highly efficient and selective since we did not detect any protein in the fractions eluted from the different control runs on U(VI)-free beads, except for the highly abundant large Rubisco subunit from leaf extracts, which was thus not considered as a U(VI)-affine protein (Supplementary Table S2). Taken together, our analyses identified a total of 338 different proteins from leaves and roots, among which 38 were specifically captured on U(VI)-loaded beads, and were named UraBP1 to 38 (Supplementary Table S2). The overall low number of total proteins identified in our analyses was the consequence of the high dilution and the small amounts of protein fractions exposed to U(VI)-loaded beads, which was a prerequisite for high selectivity and very low background noise. We considered as genuine UraBPs only proteins captured from identical AEC fractions in experiments 1 and 2, or proteins captured from different AEC fractions from the same organ (leaf or root) (highlighted in red and pink, respectively in Supplementary Table S2). Single occurrences were not considered as proteins of interest.

Among the 38 UraBPs identified, 30 were specifically captured from leaf protein extracts, 4 from root protein extracts and 4 from both tissues (Supplementary Table S2). Interestingly, 10 out of the 38 UraBPs (UraBP3, 15, 18, 21, 25, 28-31 and 33) were detected only in captured fractions and not in the flow through fractions, or were highly enriched on the captured fractions (on a spectral count basis) (Supplementary Table S2). The other UraBPs were detected similarly in both fractions and could either correspond to abundant UraBPs saturating U(VI)-loaded beads or to proteins with low uranyl binding affinity with a free/bound equilibrium being established. In order to select the most interesting UraBPs for further analyses, we performed gene ontology (GO) and semantic terms enrichment analyses (biological process and/or molecular function in relation with metals) as well as analyses of some of their physico-chemical characteristics (Supplementary Table S2). This included their content in some amino acid residues known to coordinate with U(VI) (the oxygen of aspartate, glutamate, and tyrosine and the nitrogen of histidine are both hard Lewis bases and are able to bind U(VI)). Also, phosphorylated amino acid residues that are known to interact with U(VI) and have been shown to strengthen the binding of U(VI) to aspartate and glutamate were analysed (Garai and Delangle, 2020; Laporte et al., 2019; Pardoux et al., 2012; Sauge-Merle et al., 2017; Starck et al., 2017). Firstly, these analyses indicated that most of the *Arabidopsis* UraBPs (27/38 *i.e.* 71% of the protein data set) are described as metal-binding proteins and/or are metal-responsive proteins. The phosphoproteins were also greatly represented (29/38 *i.e.* 76% of the protein data set), which is quite higher than in global proteomes (about 40-47% in *Arabidopsis*) (Mergner et al., 2020; van Wijk et al., 2014). Among phosphoproteins, 20 out of

29 were poly-phosphorylated. Particularly, UraBP17 (PSBP1), UraBP18 (BCA2), UraBP23 (RCA), UraBP25 (PCaP1), UraBP28 (PSBQ2), UraBP33 (RBG7) and UraBP38 (CATA3) contain more than five phosphorylation sites (Supplementary Table S2). Noticeably, 38% of the phosphoproteins present one or more phosphotyrosine group, which is much higher than in global *Arabidopsis* phospho-proteome (< 5%) (Mergner et al., 2020; Reiland et al., 2009; van Wijk et al., 2014).

With all these criteria taken into consideration, we decided to focus our attention more particularly onto UraBP25 for more detailed characterization. Indeed, UraBP25 is a Ca^{2+} regulatory protein that binds Ca^{2+} and Cu^{2+} ions that was previously reported as the Plasma membrane-associated Cation-binding Protein 1 (PCaP1), or the Microtubule Destabilizing Protein of 25 kDa (MDP25) (Ide et al., 2007; Li et al., 2011; Nagasaki-Takeuchi et al., 2008; Nagasaki et al., 2008; Qin et al., 2014). UraBP25 accumulates in response to Cu^{2+} and Mg^{2+} ions excess and its abundance is lowered in response to Fe^{3+} ions exposure (Ide et al., 2007; Nagata et al., 2016). Moreover, UraBP25 was isolated from both leaf and root extracts on U(VI)-loaded beads and was highly enriched in captured fractions from both R3A, R3B and L3A, L4B AEC fractions (Supplementary Table S2). Finally, UraBP25 is a poly-phosphorylated protein, with 9 identified sites, and presents a high frequency of glutamate residues (44/225 *i.e.* 19.6% of total residues) (Supplementary Table S2), compared to 6.65 % on average in the *Arabidopsis* proteome (Tsuji et al., 2010).

3.2. *PCaP1 binds U(VI) with high affinity and Cu(II) and Fe(III) in high proportions*

In order to confirm the capacity of PCaP1 from *Arabidopsis thaliana* to bind U(VI) and to further characterize its metal-binding properties, we cloned the cDNA encoding the full length PCaP1 protein by RT-PCR and produced the recombinant protein devoid of any tag sequence in *E. coli*. We used a three-step chromatographic procedure to purify recombinant PCaP1 protein to near homogeneity (Figure 2). The integrity of the preparations was confirmed by LC-ESI TOF MS under denaturing conditions. The experimental mass of PCaP1 was 24,453.06 Da, matching the amino acidic sequence 2-225 (with loss of the N-terminal methionine) (Supplementary Figure S2A). As previously observed (Ide et al., 2007), the purified protein was detected as a 36 kDa polypeptide on SDS-PAGE instead of 24.5 kDa due to its peculiar amino acid composition (Figure 2A), PCaP1 being particularly rich in glutamate, lysine and valine residues. Also, recombinant PCaP1 protein behaved as an apparent ~90 kDa globular protein by size exclusion chromatography (SEC) onto a Superdex 200 Increase 10/300 GL column, as calculated from a calibration curve obtained by measuring elution volumes of spherical folded calibration proteins (Figure 2B). However, native ESI MS analysis indicated

that PCaP1 was essentially a monomer (1mer) in solution under our assay conditions, with a small proportion of dimer (2mer) also being detected (Figure 2C). The unexpected migration of recombinant protein by SEC analysis could be explained by the occurrence of an intrinsically unstructured region in PCaP1 structure, as suggested previously by far-UV circular dichroism spectroscopy analyses (Nagasaki-Takeuchi et al., 2008).

In a previous biochemical and biophysical study, Nagasaki-Takeuchi et al. (2008) demonstrated by fluorescence titration and circular dichroism analyses that a recombinant *A. thaliana* PCaP1 protein was able to bind Cu(II) ions. These analyses indicated that binding of Cu(II) altered the structure of PCaP1 locally at proximity of aromatic amino acid residues, and particularly of Tryptophan 4 (Trp4), the unique Trp residue within the protein sequence. Here, taking advantage of this property, we checked for U(VI) binding to PCaP1 by Trp fluorescence titration. We observed that the fluorescence emission peak at 342 (typical for Trp residue exposed to a water solution) when excited at 277 nm, was also markedly quenched by the addition of U(VI) ions at low concentrations to recombinant PCaP1 protein (up to 4 equivalents on a monomer basis) buffered at pH 6, suggesting interaction of the metal with the protein (Supplementary Figure S3). Addition of an excess of EDTA restored almost completely the original fluorescence spectrum indicating reversibility of U(VI) binding and testifying of protein integrity maintenance upon U(VI) exposure. Trp fluorescence quenching was followed by titration of a 0.8 µM PCaP1-buffered solution at pH 6 containing a 12.5-fold excess of iminodiacetic acid (IDA), a well-known low affinity competitor for U(VI) binding, to control uranyl speciation (Figure 3A). The stability constants of complexes formed with IDA at pH 6 being known (Jiang et al., 2002), one can infer the conditional stability constant of the uranyl complexes with PCaP1. Under our assay conditions, the fluorescent peak at 342 nm gradually decreased with the increase in the U(VI) concentration from 0.1 to 2 µM and reached less than 20% of the original fluorescence (Figure 3A). The evolution of fluorescence intensity with the quantity of uranyl added was characteristic of the formation of a (UO_2^{2+})-$(Protein)_2$ complex, since the extrapolation of the initial slope converged to 0.5 uranyl equivalent in the complex. This was clearly confirmed in the fitting procedure (Figure 3B). Indeed, the best fit to the experimental data was obtained with a model considering a non-fluorescent (UO_2^{2+})-$(Protein)_2$ complex only, involving two proteins for one single uranyl cation. The calculated conditional stability constant for the formation of this species deduced from the deconvolution of fluorescence data was $\log\beta_{12} = 14.5 \pm 0.4$. This constant was defined for a 1:2 complex so its value has not the same order of magnitude than a $1/K_d$ value. Thus, this value cannot be compared directly with literature data reporting β_{11} constants (1:1 complex) or K_d values. To make such a comparison possible, we simulated competitions with a (UO_2^{2+})-P' complex with a theoretical competing P' protein of 1 nM affinity ($\log\beta_{11} = 9$), 10 nM ($\log\beta_{11} = 8$) or 100 nM ($\log\beta_{11} = 7$). This simulation indicated that the protein has an affinity for uranyl similar to a

protein having a 10 nM affinity ($\log\beta_{11}$ = 8) in a (UO_2^{2+})-P' complex, using a similar approach (Supplementary Figure S4). Trp fluorescence quenching was also followed by titration of a PCaP1-buffered solution at pH 7.5 (Supplementary Figure S5A). The evolution of fluorescence intensity with the quantity of uranyl added could not be easily interpreted since there was no plateau with an addition of a large amount of U(VI) up to 20 µM (Supplementary Figure S5B). So, fits were not appropriate under these conditions.

To study the stoichiometry of U(VI) complexation to PCaP1 at pH 6 and 7.5, we determined U(VI) content by ICP-MS in U(VI)-PCaP1 complexes formed after incubation of 10 µM PCaP1-buffered samples in the presence of 50 µM uranyl nitrate (5 U(VI) equivalents). Separation of complexes from unbound metal was achieved through centrifugation onto Sephadex MicroSpin G-25 columns. We did not perform such analyses at higher U(VI) to protein ratios since under large U(VI) excess conditions, protein samples were somewhat affected, as monitored by UV-Vis absorption, and a slight precipitate was observed, particularly when titration was done in MES buffer at pH 6 (not shown). Under optimized conditions, data obtained revealed a ligand-binding number of 0.50 ± 0.03 U(VI) ions per PCaP1 monomer at pH 6 (Supplementary Table S3), in line with fluorescence spectroscopy studies (Figure 3B). Since PCaP1 was found to be mainly a monomer in solution (Figure 2C), these data could suggest dimerization of the protein upon U(VI) exposure under our experimental conditions, with one uranyl cation located at the interface of two monomers (compatible with formation of a 1:2 complex, in line with fluorescence titration experiments; Figure 3B). When performed at pH 7.5 in Tris-HCl buffer, binding experiments revealed a U(VI) content of the resulting U(VI)-protein complex of 2.11 ± 0.07 U(VI) ions per PCaP1 monomer (Supplementary Table S3).

As mentioned before, Nagasaki-Takeuchi et al. (2008) characterized Cu(II)-binding properties of PCaP1 by fluorescence titration of Trp4 with $CuCl_2$ increasing concentrations and monitoring of changes in fluorescence spectra. The obtained values of apparent K_d ($K_d$app) and ligand-binding number, as determined by indirect fluorescence and absorption spectroscopy methods, were 10 to 16 µM and 6 to 7 Cu(II) ions per monomer, respectively (Nagasaki-Takeuchi et al., 2008). In our hands, under similar assay conditions, the fluorescence emission peak at 342 nm was also markedly quenched when Cu(II) was added in the protein solution, at concentrations up to 300 µM (Supplementary Figure S6A). From the collected data we calculated a $K_d$app for Cu(II) binding of 29 µM, and a ligand-binding number of 13 ions per monomer (Supplementary Table S4).

PCaP1 has been shown to interact with calcium and calmodulin in a calcium-dependent manner and has both *in vitro* and *in vivo* calcium-dependent microtubule destabilizing and actin severing activities (Li et al., 2011; Nagasaki et al., 2008; Qin et al., 2014). Despite PCaP1 being a genuine Ca(II)-binding protein, thus requiring calcium for its activities, we observed that the addition of $CaCl_2$ has a limited effect on fluorescence emission, at pH 7.5. However,

fluorescence changes were significant at pH 5.5, yielding a $K_d$app of 241 µM (Supplementary Figure S6B and Supplementary Table S4). Interestingly, Fe(III) but not Fe(II) ions also affected Trp fluorescence emission in a similar way as Cu(II) ions ($K_d$app of 26 µM and ligand-binding number of about 19 ions per monomer; Supplementary Figure S6C and Supplementary Table S4). Finally, none of the other metal ions tested had any impact on fluorescence emission (Supplementary Table S4). In order to confirm the ability of PCaP1 to bind Cu(II), Ca(II) and Fe(III) ions, we used SEC on MicroSpin G-25 columns and ICP-MS analyses to measure metals in protein complexes resulting from the incubation of 10 µM PCaP1 with large excess of any of the metal ions. Data obtained revealed an apparent stoichiometry for Cu(II)-PCaP1 protein complexes of 15:1, consistent with the values estimated by fluorescence spectroscopy. Surprisingly, much higher values were observed by direct ICP-MS determination for Fe(III)-PCaP1 protein complexes (stoichiometry of 60:1 compared to 19:1 by fluorescence spectroscopy; Supplementary Table S4). Unfortunately, we were unable to measure accurately the calcium content of Ca(II)-PCaP1 protein complexes because of unexplained high background values of unbound metal ion in MicroSpin G-25 column eluates.

PCaP1 is known to bind the physiological ion Ca(II) both *in vivo* and *in vitro* (Li et al., 2011; Nagasaki et al., 2008; Qin et al., 2014). However, we have shown that at physiological pH (pH 7.5), Ca(II) alone did not significantly quench PCaP1 fluorescence (Supplementary Table S4), therefore a competition between UO_2^{2+} and Ca(II) could be evidenced by an increase in Trp fluorescence intensities of U(VI)-PCaP1 protein complexes upon addition of increasing Ca(II) concentrations (Supplementary Figure S7). Thereby, addition of 8 mM Ca(II) fully restored Trp fluorescence intensity of PCaP1 protein initially quenched to half its initial value by 20 µM U(VI), which suggested identical or close binding-sites for both metals and indicated a much higher affinity of the protein for U than for calcium, even at physiological pH.

3.3. *U(VI)-binding to PCaP1 induces oligomerization*

In order to obtain information about the *in vitro* interaction of U(VI) with PCaP1 at the molecular level, we initiated structural studies of the complex. The recombinant protein was predicted to be an instable protein (Instability Index of 53.55 using ProtParam tool; Supplementary Table S2) due to the presence of a long intrinsically disordered C-terminal domain (residues 140-225, as identified by computational disorder prediction tools) (Supplementary Figure S8A). All our attempts to crystallize PCaP1 were unsuccessful, most likely because of this high degree of flexibility. Consequently, structure determination based on X-ray crystallographic data was not pursued. As an alternative strategy, we have undertaken solution-state NMR spectroscopic analyses of this protein. Solution-state NMR spectroscopy is a well-adapted technique for low molecular weight proteins (< 30 kDa), which is the case for PCaP1, providing information about

structure and conformational dynamics of proteins over a wide range of time scales and degrees of order. NMR experiments require samples at high protein concentration (typically > 100 µM), for which U(VI) exposure triggers precipitation of PCaP1 at pH 6, but not at pH 7.5. Thus, all NMR experiments were performed at pH 7.5 with U(VI):protein ratios in the range between 0:1 to 5:1.

The 1D ^{1}H NMR spectrum of PCaP1 shows a few backbone amide (HN) and side-chain methyl (CH_3) NMR resonances outside the typical random-coil region, indicative of the presence of well-folded protein segments (Supplementary Figure S8B). In addition, a more quantitative assessment of the degree of tertiary structure in PCaP1 using the HETSOFAST approach (Schanda et al., 2006) confirmed the presence of both well-folded domains and flexible protein regions (Supplementary Figure S8C).

In order to obtain site-specific information on the structural and dynamic properties of recombinant PCaP1, we produced uniformly ^{13}C,^{15}N-labeled PCaP1 and performed a set of 3D NMR assignment experiments (Best-TROSY HNCO, HNCACO, HNCA, HNCOCA, HNCACB and HNCOCACB) (Favier and Brutscher, 2011; Solyom et al., 2013). Based on this data set, 85% of the non-proline PCaP1 residues were unambiguously assigned (Figure 4A; Supplementary Figure S9A). The assigned chemical shifts revealed the presence of a N-terminal structured domain (residues 29-129), mainly formed by α-helices, and a highly flexible (intrinsically disordered) C-terminal domain (residues 132-225) (Figure 4B; Supplementary Figure S9A). We did not intend an atomic-resolution structure determination by NMR, but rather computed a structural model with AlphaFold2, a DeepMind AI-based computational tool that was proven to produce accurate structural models for the majority of the protein targets tested (Jumper et al., 2021). The resulting AlphaFold2 structural model (Figure 4C) presents all the secondary structural features (α-helical structure) that have been derived from our NMR data, providing an independent validation of this computational model.

The 2D ^{1}H-^{15}N correlation spectra of PCaP1 recorded in the presence of increasing amounts of U(VI) resulted in a progressive decrease of peak intensities for residues located in the structured N-terminal part, while no such intensity loss was observed for the highly flexible C-terminal segment (Figure 5A). In contrary, some amide sites in this flexible part even gained in NMR signal intensity. Interestingly, no changes in peak positions were observed during this NMR titration experiment. These findings suggest that the structured N-terminal part of PCaP1 oligomerizes upon U(VI) binding. In order to obtain a more quantitative idea about the average particle size in PCaP1:U(VI) mixed samples, we performed NMR-based translational diffusion experiments. The intensity decay of observed ^{1}H signals, mainly corresponding to the flexible C-terminal domain, as a function of the applied gradient-field strength are plotted in Figure 5B for U(VI):PCaP1 ratios of 0:1; 1:1 and 5:1. The translational diffusion constants extracted from these curves are 21% (1:1) and 42% (5:1) smaller in the presence of U(VI) as compared to the

diffusion of the free PCaP1 protein. This apparent slower diffusion corresponds to an average particle size that is increased 2 and 5-fold for the 1:1 and 5:1 mixtures, respectively.

In the case of a 1:1 stoichiometric ratio, we observed a decrease in signal intensity in the ^{1}H-^{15}N spectrum by a factor 2 for the structured part of the protein (Figure 5C). In view of our translational diffusion results, this reduced signal intensity may originate either from the presence of U(VI)-bound PCaP1 dimers, or free PCaP1 in slow exchange (high binding affinity) with larger PCaP1 oligomers that are invisible by NMR. In order to discriminate the two scenarios, we performed ^{15}N spin relaxation experiments that provide quantitative information about changes in rotational tumbling correlation times upon interaction with U(VI). Site-specific ^{15}N relaxation rate constants T_2 and T_1, measured for free PCaP1 and a 1:1 U(VI):PCaP1 mixture (Figure 5C), did not show any significant difference for the structured N-terminal part. This observation is in agreement with a model of coexisting monomeric and oligomeric species with only the free PCaP1 monomers contributing to the detected NMR signal. In an attempt to detect additional NMR signals in the ^{1}H-^{15}N correlation spectra, arising from U(VI)-bound PCaP1 oligomers, we produced ^{2}H,^{15}N-labeled PCaP1 protein (deuterated to about 70%) to reduce spin-relaxation-induced NMR signal loss. However, even under these isotope-labeling conditions favorable for the detection of more slowly tumbling molecules, no additional peaks could be observed in an overnight experiment, strongly suggesting that the undetected species correspond to relatively large oligomers (at least trimers or tetramers).

Surprisingly, for some peptide regions in the flexible C-terminal part of PCaP1, notably around residue 160, we observed a significant increase in NMR signal intensity upon uranyl binding (Figures 5A, C). Note that the corresponding ^{1}H-^{15}N correlation peaks for these residues were of (very) low intensity in the spectra of free PCaP1, most likely due to conformational exchange-induced line broadening effects (dynamics on the µs – ms time scale). ^{15}N relaxation rates (T_1 and T_2) indicated only minor changes in the local dynamics on the fast (sub-ns) time scale. In particular, the high T_2 and low T_1 values confirmed that this domain remains highly flexible in the presence of uranyl. The observed increase in signal intensity upon uranyl binding for the peptide region around residue 160 can thus be explained either by a side effect of U(VI)-binding to the structured N-terminal part, altering the dynamic properties of this peptide region, or by additional binding site(s) in the C-terminal part of PCaP1, again inducing a change in the local dynamics of the peptide chain.

3.4. *U(VI) binds to the structured N-terminal and disordered C-terminal domains of PCaP1*

In an attempt to better understand the interaction of U(VI) with the structured and disordered parts of the protein, we produced two truncated forms of PCaP1, deleted from all or part of the flexible region of the protein (Supplementary Figure S2B, C). The first one was a minor splicing

variant of PCaP1, formed by cryptic intron splicing within exon 4 (herein named PCaP1v), that was isolated in the course of PCR-cloning of the full-length ORF (this form represented 1/10th of the clones obtained by PCR cloning). This cDNA encodes a PCaP1 protein form lacking residues 172-212 (Supplementary Figure S9B). The second PCaP1 form produced (herein named PCaP1Δ) was designed to remove the whole C-terminal flexible domain (residues 143-225). The structural integrity of the PCaP1Δ construct was checked by NMR spectroscopy, with no (significant) spectral changes in the ^{1}H-^{15}N correlation spectrum of PCaP1Δ with respect to N-terminal residue signals detected in the spectrum of the full-length protein (Supplementary Figure S10A). No degradation of recombinant proteins was also noted, as judged by SDS-PAGE analysis and mass spectrometry in denaturing conditions (Supplementary Figure S2).

The stoichiometry of U(VI) complexation to both PCaP1v and PCaP1Δ forms was analyzed by MicroSpin G-25 chromatography coupled to ICP-MS, at pH 6 and 7.5 under the same conditions as for full-length PCaP1 (Supplementary Table S3). Data obtained for PCaP1v were very close to those observed for PCaP1, (*i.e.* 0.5 U(VI)/monomer at pH 6 and ~2 U(VI)/monomer at pH 7.5), demonstrating full U(VI)-binding capacity of this truncated protein. Concerning PCaP1Δ, data obtained at pH 6 were also similar to those measured for the other two forms (0.56 U(VI)/monomer). At pH 7.5, however, the U(VI)-binding capacity of PCaP1Δ was at least reduced by 2 times (≤ 1 U(VI)/monomer), as compared to that of the other forms. Trp-fluorescence titration of PCaP1v by up to 2 U(VI) equivalents at pH 6 gave quenching spectra profiles similar to those of the full-length PCaP1 protein (Supplementary Figure S11A), yielding a calculated conditional stability constant for U(VI) complex ($UO_2(P_2)$ model) $\log\beta_{12}$ = 14.2 ± 0.7, close to that measured for the full-length PCaP1 protein (Supplementary Table S5). In contrast, the fluorescence spectrum of PCaP1Δ was altered and fluorescence intensities were too low to determine a conditional stability constant (Supplementary Figure S11B; Supplementary Table S5).

NMR titration experiments adding increasing amounts of U(VI) to a sample of PCaP1Δ showed a shift in binding stoichiometry with respect to full-length PCaP1 (Supplementary Figure S10B, C). At sub-stoichiometric amounts of U(VI) the NMR signal intensity decreased, without changing the translational diffusion properties of the NMR-observable species (similar to full length PCaP1), while no NMR signal was detected for U(VI):PCaP1Δ ratios as soon as uranyl was provided in excess. A SEC analysis of PCPa1Δ protein exposed to a 5-fold excess U(VI), using a Superdex 200 10_30 Increase GL column, showed that protein completely eluted as large oligomers under these conditions, while the free protein behaved as a monomer (Supplementary Figure S12). The NMR signal was partly recovered by adding EDTA (5 mM),

suggesting that U(VI) induced PCaP1Δ oligomerization can be reversed by U(VI)-EDTA complexation (not shown).

3.5. U(VI) translocation in Arabidopsis shoots is affected in a pcap1 null-mutant

Our data showed that PCaP1 has the capacity to bind U(VI) with high affinity at various sites, *in vitro*. In order to determine a possible involvement of PCaP1 on the fate of U(VI) *in planta*, we obtained Arabidopsis seeds of an homozygous T-DNA insertion line of PCaP1 (*mdp25*; Li et al. (2011); also known as *pcap1-4*; Nagata et al. (2016); herein named *knock-out* (*ko*) mutant). Also, we generated transgenic lines expressing the full-length PCaP1 under the control of a 35S promoter in the *ko* mutant line background (*ko/35S::PCaP1* lines). Three independent homozygous transgenic lines carrying the *35S::PCaP1* construct, among the 9 obtained, were selected for subsequent U(VI) uptake and translocation analyses (#2; #10 and #30 lines). A western blot analysis of total shoot proteins using a PCaP1 antibody showed no detectable PCaP1 protein in the *ko* mutant, confirming that it is a genuine null-mutant (Figure 6A; Nagata et al. (2016)). Transgenic lines exhibited nearly wild-type levels of PCaP1 expression. To estimate the importance of PCaP1 synthesis on the accumulation of U(VI), plants were grown for 4 weeks in a complete standard Gre medium, then transferred in a Gre medium depleted of Pi and exposed to 20 µM uranyl nitrate for short (1 or 2 days) and long (11 days) periods of time. No obvious difference was observed on plant growth between the different lines, for the same U(VI) exposure time (not shown). We used the photosynthetic parameter Fv/Fm (measurement of photosystem II efficiency in dark-adapted leaves) as an estimate of plant fitness, and found it was unchanged in all cases (comprised between 0.79 ± 0.01 and 0.81 ± 0.01). Root and shoot U(VI) content was determined by ICP-MS following careful washing of plant tissues with sodium carbonate and deionized water to eliminate the loosely-bound radionuclide. In agreement with previous observations made under comparable conditions (Berthet et al., 2018; Doustaly et al., 2014; Saenen et al., 2014; Sarthou et al., 2022; Vanhoudt et al., 2008), the amount of U(VI) in shoots was low compared to roots in wild-type (Col-0) control plants, with an highest translocation factor (shoot to root ratio) of 6×10^{-3}, illustrating the low mobility of U(VI) in Arabidopsis (Figure 6B, C). Data presented in Figure 6B showed that U(VI) biosorption in roots was poorly affected in *pcap1 ko* plants or in transgenic lines as compared to Col-0 control plants, throughout the experiment. In contrast, U(VI) translocation in Arabidopsis shoots was significantly affected in *ko* plants after 11 days of U(VI) exposure, as compared to Col-0 controls, showing a 2 to 3-fold decrease in U(VI) translocation (Figure 6C). No difference was observed for short periods of U(VI) exposure (days 1 or 2). Finally, ectopic expression of PCaP1 cDNA in *pcap1 ko* plants (#2, #10, #30 transgenic lines)

restored wild-type levels of U(VI) translocation in shoots, in line with PCaP1 protein expression levels.

4. Discussion and conclusions

The cellular toxicity of U(VI) in prokaryotic and eukaryotic organisms is not yet fully described but it likely results from its ability to bind strongly to biomolecules, mainly proteins that contain numerous uranyl-binding groups. Over the past few years, significant progress has been made in identification of UraBPs from various organisms, including the hyperthermophilic archaea *Pyrococcus furiosus* (Cvetkovic et al., 2010), the crayfish *Procambarus clarkii* (Xu et al., 2014), the zebrafish *Danio rerio* (Bucher et al., 2014; Eb-Levadoux et al., 2017), rat (Frelon et al., 2009) and humans (Basset et al., 2008; Dedieu et al., 2009; Huynh et al., 2015; Vidaud et al., 2005; Vidaud et al., 2019). These proteins were identified by a combination of non-denaturing electrophoretic and/or chromatographic approaches combined with proteomic analyses, allowing to isolate proteins with affinity for U(VI) either *in vitro*, *in cellulo* or both.

Despite U(VI) is known to be taken up by plants and to have cellular toxic effects, very few of the proteins involved in these processes have been identified so far (Berthet et al., 2018; Doustaly et al., 2014; Laurette et al., 2012; Misson et al., 2009; Serre et al., 2019; Vanhoudt et al., 2011). Recently, several evidences were provided that U(VI) is taken up by the roots of Arabidopsis plants through MCA1 and ANN1 Ca^{2+}-permeable cation channels (Sarthou et al., 2022). However, the fate of U(VI) within plant cells is still largely unknown. In particular, identification and characterization of UraBPs have not been done so far in higher plants or any photosynthetic organism. Here, in order to identify UraBPs in Arabidopsis, we used an immobilized metal affinity chromatography (IMAC) method, based on the cation-exchange properties of aminophosphonate groups for U(VI) binding (Basset et al., 2008). Such a technique was developed because uranyl cations have singular physico-chemical characteristics that prevent them from being immobilized on commercially available metal chelating supports. This IMAC technique was a powerful tool for capturing UraBPs *in vitro*, from human serum (Basset et al., 2008), kidney-2 cell extracts (Dedieu et al., 2009) and dopaminergic SH-SY5Y cells (Vidaud et al., 2019). Adapted to plant soluble protein extracts, this technique allowed us to capture and identify 38 UraBPs from Arabidopsis shoots and/or roots. Interestingly, several proteins identified in our study are homologous to UraBPs identified in other organisms. For example, the glycolytic enzymes fructose-bis phosphate aldolases 2 and 1 (UraBP7 and 13, in this study) are homologous to several aldolases identified in human urano proteomes (Dedieu et al., 2009; Vidaud et al., 2019). Also, peroxiredoxin Q (UraBP29), the plasma-membrane associated cation-binding protein, PCaP1 (UraBP25) and the glycine-rich RNA-binding protein 7 (UraBP33) are related to peroxiredoxin 1, the numerous actin network regulatory proteins, and various ribonucleoproteins, identified

in the human urano proteomes, respectively (Dedieu et al., 2009; Vidaud et al., 2019). Finally, the beta carbonic anhydrase 2 (UraBP18) and the glutathione S-transferase F2 and F7 (UraBP15 and 35) are homologous to carbonic anhydrase and glutathione S-transferases, respectively, identified as UraBPs in zebrafish and the crayfish (Bucher et al., 2016; Eb-Levadoux et al., 2017; Xu et al., 2014).

Among the 38 UraBPs identified in this study, we focused on PCaP1 for a detailed characterization. PCaP1 was previously shown to bind calcium possibly at a unique site and copper at multiple sites, both *in vitro* and *in planta* (Ide et al., 2007; Nagasaki-Takeuchi et al., 2008; Nagasaki et al., 2008; Nagata et al., 2016; Qin et al., 2014). Here, we established that recombinant PCaP1 was indeed able to bind copper but also ferric ion to multiple sites. The large number of glutamate residues in the protein sequence and particularly in the intrinsically unstructured region probably accounted for this high-capacity metal binding. We also demonstrated that PCaP1 was able to bind U(VI) with high affinity, and that calcium somewhat competed with U(VI) for binding. At pH 6, PCaP1 displayed high U(VI)-binding affinity with a conditional dissociation constant in the vicinity of 10 nM. By comparison, binding constants for U(VI) of the same order (from the sub-nanomolar to the sub-micromolar range) were reported for peptides or proteins with native or artificial metal-binding sites, using similar experimental approaches (Acharya and Blindauer, 2016; Basset et al., 2013; Gallois et al., 2021; Laporte et al., 2019; Le Clainche and Vita, 2006; Lebrun et al., 2014; Michon et al., 2010; Pardoux et al., 2012; Qi et al., 2014; Sauge-Merle et al., 2017; Starck et al., 2017; Starck et al., 2015; Wegner et al., 2009), and also reviewed by Lin (2020).

In a more singular way, our results are consistent with U(VI) exposure inducing PCaP1 oligomerization. Structural impacts of U(VI) binding to proteins reported in the literature vary from slight secondary structural to large conformational changes, but to our knowledge, no study describes a change of protein oligomeric state (Acharya and Blindauer, 2016; Bal et al., 2013; Basset et al., 2013; Gallois et al., 2021; Hoarau et al., 2019; Lin et al., 2011; Pardoux et al., 2012; Qi et al., 2014; Sun et al., 2014; Vidaud et al., 2007; Wan et al., 2012; Zhou et al., 2014).

Structural evidences indicate that the presence of two oxo groups in uranyl cation promotes the coordination of four to six additional ligands to U(VI) in its equatorial plane perpendicular to the O-U-O axis (Garai and Delangle, 2020; Van Horn and Huang, 2006). In this context, based on the results obtained on the full-length and truncated versions of PCaP1 by fluorescence titration, U(VI) quantification by ICP-MS, solution-state NMR and SEC analyses, we can suggest structural models for the interaction with uranyl (Figure 7). At pH 6, our data are consistent with the occurrence of one U(VI)-binding site at the interface of two monomers and coordinated by residues from the two monomers, yielding a stoichiometry of the complex of 0.5 U(VI)/monomer (in line with the 1:2 model fitting the fluorescence titration data) (Figure

7A). Such a stoichiometry in U(VI)-PCaP1 complex was found in all the protein forms analyzed (PCaP1, PCaP1v and PCaP1Δ) (Supplementary Table S3), suggesting that the U(VI)-binding site is located at the surface of the structured domain. At pH 7.5, the situation is more complex. According to our data, the well-folded N-terminal domain of PCaP1 possesses (at least) two high-affinity uranyl binding sites. Uranyl binding occurs at the interface between two monomers, thus allowing the formation of oligomers of different size and shape. The average stoichiometry U(VI):PCaP1 of such large oligomers is 1:1 (Figure 7B). The disordered C-terminal domain also possesses one or several uranyl binding sites of similar affinity than the N-terminal domain. Our study highlights the peptide segment around residue 160 to be involved in uranyl binding, as PCaP1v, retains the uranyl binding features of the full-length protein, and NMR shows altered conformational dynamics in this region upon uranyl binding. In the full-length protein, the flexible C-terminus is responsible for scavenging part of the available U(VI), which explains our results showing that about twice as much U(VI) is required to observe the complete disappearance of NMR signals from the well-folded monomeric N-terminal part of the full-length PCaP1 protein than of the isolated N-terminal domain. Uranyl-binding by the disordered C-terminal domain most likely induces the formation of a highly dynamic mesh of peptide chains, which contributes to the larger apparent particle size of U(VI)-PCaP1 complexes (Figure 5B). Such a configuration would be consistent, as observed, with a mean global U(VI) content for large complexes close to or higher than 2 U(VI)/monomer of full-length protein (about 1 U(VI) equivalent per structured domain and 1 U(VI) equivalent per unstructured domain) (Figure 7 B).

The capacity of PCaP1 to bind U(VI) *in vitro* does not provide insight into the functional, physiological and developmental consequences of protein-metal interactions *in planta*. PCaP1 is located on the inner side of the plasma membrane *via* N-myristoylation of the glycine 2 residue (Ide et al., 2007; Nagasaki et al., 2008; Nagata et al., 2016). At first glance, one would expect PCaP1 to prevent the diffusion of U(VI) into the cells and protect the plant from its toxic effects. This prediction is strengthened by the fact that PCaP1 is poly-phosphorylated *in vivo* (Supplementary Table S2; (Mattei et al., 2016; Rayapuram et al., 2014)), a situation known to amplify the affinity of proteins for U(VI) (Laporte et al., 2019; Qi et al., 2014; Starck et al., 2017; Starck et al., 2015). Such scavenging of U by a high-affinity protein to prevent its toxic outcomes would resemble that described for the UipA protein in U(VI)-tolerant *Microbacterium* species. UipA is a single-pass transmembrane protein exposed to the external phase of the plasma membrane; it is induced by U(VI) and protects *Microbacterium* from U(VI) entry thanks to the high affinity of its large soluble domain for U(VI) (Gallois et al., 2021). However, the role of PCaP1 does not resemble that of UipA. Indeed, the absence of PCaP1 in *pcap1-null* mutants has no impact on U(VI) accumulation in roots as compared with wild-type plants. On the contrary, the presence of wild-type levels of PCaP1 seemes to promote translocation of U(VI)

from roots to aerial parts (Figure 6). In Arabidopsis, PCaP1 was found to regulate the actin (severing activity) and the microtubule (depolymerizing activity) cytoskeleton in a calcium-dependent manner (Li et al., 2011; Qin et al., 2014). PCaP1 was also proposed to play a role in calcium signaling through its binding to calmodulin and phosphatidylinositol phosphates (Kato et al., 2010; Nagasaki et al., 2008). In connection with these activities, PCaP1 negatively regulates hypocotyl elongation (Li et al., 2011), pollen-tube growth (Qin et al., 2014), and the root hydrotropic response (Tanaka-Takada et al., 2019). Moreover, it is involved in plasmodesmata aperture associated to plant immunity (Cheng et al., 2020; Giovannoni et al., 2021; Vijayapalani et al., 2012) and stomatal closure (Nagata et al., 2016). These structures have a key role in the transport of small molecules and ion for cell-to-cell communication (Roeder et al., 2022) and in water and metabolites fluxes into the xylem through the driving force of transpiration (Hetherington and Woodward, 2003). It is conceivable that perturbation of these mechanisms by inactivation of the *PCaP1* gene might be responsible for the observed defect in U(VI) translocation. Further work is needed to determine precisely by which mechanism PCaP1 favors U(VI) translocation to shoots and if the peculiar U(VI)-binding properties of the protein is involved in this process, particularly given the apparent much higher affinity of the protein for U(VI) than for calcium at the slightly alkaline pH of plant cell cytosol.

Statement of environmental implication

Uranium (U) is a harmful radionuclide that may be absorbed by plants from soil and, consequently, contaminate the food chain, with human and animals health hazards. The cellular toxicity and detoxification mechanisms of U are still poorly described but likely result from its ability to bind strongly to biomolecules, mainly proteins. Our study describes for the first time the large-scale identification of U-binding proteins from plant tissues and the further characterization of one of them both *in vitro* and *in planta*. Our findings represent an important milestone to advance knowledge in the fields of radionuclide toxicology and phytoremediation.

Data availability

All data supporting the findings of this study are included in this published article (and its Supplementary Information files), or are available from the corresponding authors upon reasonable request. NMR chemical shifts of PCaP1 have been deposited with the BMRB (http://www.bmrb.wisc.edu/) under accession number 51607.

Sequence data from this article can be found in the GenBank/EMBL, Arabidopsis Genome Initiative and/or UniProt databases under the following accession numbers: PCaP1 (At4g20260; Q96262); PCaP1v (splicing variant; ON209435).

The proteomics data have been deposited to the ProteomeXchange Consortium via the PRIDE (Perez-Riverol et al., 2019) partner repository with the dataset identifier PXD033354 and

10.6019/PXD033354. [The dataset is available with the Username: reviewer_pxd033354@ebi.ac.uk and Password: 62dQFqjg].

CRediT authorship contribution statement

Alicia Vallet: Conceptualization, Investigation, Methodology, Formal analysis, Validation. **Jacqueline Martin-Laffon**: Investigation, Methodology, Formal analysis. **Adrien Favier:** Conceptualization, Investigation, Methodology, Formal analysis, Validation. **Benoît Revel:** Investigation. **Titouan Bonnot:** Investigation. **Claude Vidaud:** Conceptualization, Investigation, Methodology, Formal analysis, Validation, Writing – review & editing. **Jean Armengaud:** Conceptualization, Investigation, Methodology, Formal analysis, Validation, Writing – review & editing. **Jean-Charles Gaillard:** Investigation. **Pascale Delangle:** Methodology, Formal analysis, Validation, Writing – review & editing. **Fabienne Devime:** Investigation. **Sylvie Figuet:** Investigation. **Nelson Serre:** Investigation. **Elisabetta Boeri Erba:** Investigation, Methodology, Formal analysis, Validation. **Bernhard Brutscher:** Conceptualization, Methodology, Formal analysis, Validation, Writing – review & editing. **Stéphane Ravanel:** Conceptualization, Methodology, Formal analysis, Validation, Writing – review and editing. **Jacques Bourguignon:** Funding acquisition, Project administration, Conceptualization, Formal analysis, Validation, Writing – review & editing. **Claude Alban:** Funding acquisition, Supervision, Project administration, Conceptualization, Investigation, Methodology, Formal analysis, Validation, Writing – original draft, review & editing.

Declaration of Competing Interest

The authors declare that they have no known competing financial interests or personal relationships that could have appeared to influence the work reported in this paper.

Acknowledgments

This work was funded by a grant from the Toxicology Program of the CEA and grants from the Agence Nationale de la Recherche (ANR-17-CE34-0007, GreenU Project; ANR-17-EURE-0003, CBH-EUR-GS). Mélanie Robert and Isabel Ayala are kindly acknowledged for their technical assistance. We thank Dr Luca Signor for mass spectrometry analyses of recombinant PCaP1 proteins in denaturing conditions. This work used the mass spectrometry and high-field NMR platforms of the Grenoble Instruct-ERIC center (ISBG; UAR 3518 CNRS-CEA-UGA-EMBL) within the Grenoble Partnership for Structural Biology (PSB), supported by FRISBI (ANR-10-INBS-0005-02) and CBH-EUR-GS (ANR-17-EURE-0003). Financial support from the IR-RMN-THC FR3050 CNRS for conducting the research is also gratefully acknowledged.

Figure legends

Figure 1: Strategy for the isolation and identification of uranyl-binding proteins from *Arabidopsis thaliana*.

Figure 2: Purification of recombinant PCaP1 and determination of its oligomerization state. A- Documentation of PCaP1 purification. Polypeptides were separated by SDS-PAGE 12% and stained with Coomassie Brilliant Blue R250. Lane 1: soluble proteins (25 µg) from *E. coli* Rosetta cells harboring pET28-PCaP1 construct grown in the presence of IPTG; Lane 2: ammonium sulfate 50% of saturation precipitating fraction (25 µg); Lane 3: BioGel HTP hydroxyapatite column pool (15 µg); Lane 4: EMD-DEAE column pool (10 µg); Superdex 75 column pool (8 µg); M, molecular mass markers. B- Apparent molecular mass estimation of native recombinant PCaP1 by gel filtration. Purified protein (150 µg) was resolved by size exclusion chromatography (SEC) onto a Superdex 200 Increase 10/300 GL column. Eluted fractions were analyzed by SDS-PAGE. Standard proteins for column calibration (inset) were ferritin (440 kDa), covalbumin (75 kDa), carbonic anhydrase (29 kDa), and ribonuclease A (13.7 kDa). K_{av} = (Ve-Vo)/(Vt-Vo); Ve, elution volume; Vo, void volume; Vt, total volume. C- Native mass spectrum of recombinant PCaP1. 1mer (monomer) = 24453 Da; 2mer (dimer) = 48906 Da.

Figure 3: Fluorescence emission spectrum analysis of uranyl binding to PCaP1 at pH 6. A- Fluorescence titration of recombinant PCaP1 (0.8 µM) with UO_2^{2+} (0 to 2.5 equivalents) at pH 6 in MES buffer 10 mM, NaCl 100 mM, in the presence of IDA 10 µM, with excitation at 277 nm. B- Variation of the intensity at the peak maximum (342 nm) upon UO_2^{2+} addition. Circles represent experimental (Exp) values and the solid line the best fit with the program SPECFIT, taking into consideration the known conditional stability constants of the uranyl complexes with IDA. n_{eq}(U), number of U(VI) equivalents ([U(VI)]/[PCaP1]).

Figure 4: NMR assignment and structural features of PCaP1. A- Amide ^{1}H-^{15}N correlation spectrum of free PCaP1. Resolved cross peaks are annotated by their residue type (one letter amino acid code) and residue number. Sample: PCaP1 300 µM in Tris-HCl 10 mM pH 7.5, NaN_3 0.03%. B- Helical propensity along the PCaP1 backbone (only the structured part is shown) computed from the measured ^{13}C chemical shifts using the TALOS-N server (https://spin.niddk.nih.gov/bax/software/TALOS-N/). The helical elements derived from this plot (red bars) are in agreement with the structure predicted by Alpha Fold v2.0 (https://alphafold.ebi.ac.uk/) shown in (C). Model confidence (pLDDT score) for the structured domain was >90 (highly confident).The image was produced using PyMOL (DeLano Scientific, San Carlos, CA, USA) as a ribbon model colored in the “chainbows” mode.

Figure 5: NMR characterization of PCaP1-U(VI) interaction. A- Overlay of 2D ^{1}H-^{15}N correlation spectra of free ^{15}N-^{13}C labelled PCaP1 (100 µM) alone (black) or in complex (100 µM) with U(VI) (500 µM) (red) in Tris-HCl 10 mM pH 7.5. Only correlation peaks in the random

coil ^{1}H spectral region (indicated by dashed lines) remain visible upon U(VI) binding. B- Diffusion ordered spectroscopy (DOSY) measurements of PCaP1 in the absence or in the presence of 1 or 5 U(VI) equivalents. The observed NMR signal intensity (integrated over the 1D ^{1}H spectrum) is plotted as a function of the applied gradient strength. Fitting of decay curves yields the translational diffusion constant. Translational diffusion of PCaP1 decreases U(VI) with increasing amounts of uranyl, indicating the formation of larger particles. C- ^{15}N spin relaxation rate constants (T_1 and T_2) measured for free PCaP1 (black) and PCaP1 in the presence of an equal amount of U(VI) (red). In addition, the intensity ratios of ^{1}H-^{15}N correlation peaks detected in the absence and presence of an equal amount of U(VI) are plotted (top panel).

Figure 6: Uranium content in wild type, *pcap1*-null mutant and transgenic lines expressing PCaP1. Wild type (Col-0), *pcap1*-null mutant (*ko*) and transgenic lines expressing PCaP1 under the control of a 35S promoter (#2; #10 and #30 lines) were grown hydroponically for 5 weeks in Gre medium, and then challenged with 20 µM uranyl nitrate for 1, 2 and 11 days in Gre medium with no phosphate. A- Western blot analysis of total shoot proteins with a PCaP1 antibody. B- Accumulation of U in roots. C- Accumulation of U in shoots. Samples were dehydrated, digested with HNO_3, and ^{238}U was measured by ICP-MS. Data distribution is displayed in Tukey's boxplots with the median as the solid line inside the box, and the first and third quartiles as the bottom and top lines of the box, respectively. Outliers are shown as individual dots. Each distribution in boxplots represents n = 4 samples for roots and n = 4-8 samples for shoots. Statistical significance determined using non-parametric comparisons with Tukey's test is shown: *, $p < 0.05$; **, $p < 0.01$.

Figure 7: Models for *in vitro* U(VI)-PCaP1 complexes formation at pH 6 and pH 7.5.

Appendix A. Supporting information

Supplementary data associated with this article can be found in the online version.

References

Acharya, C., Blindauer, C.A., 2016. Unexpected Interactions of the Cyanobacterial Metallothionein SmtA with Uranium. Inorganic chemistry. 55 (4), 1505-1515. https://doi.org/10.1021/acs.inorgchem.5b02327

Aranjuelo, I., Doustaly, F., Cela, J., Porcel, R., Muller, M., Aroca, R., Munne-Bosch, S., Bourguignon, J., 2014. Glutathione and transpiration as key factors conditioning oxidative stress in Arabidopsis thaliana exposed to uranium. Planta. 239 (4), 817-830. https://doi.org/10.1007/s00425-013-2014-x

Bal, W., Sokolowska, M., Kurowska, E., Faller, P., 2013. Binding of transition metal ions to albumin: sites, affinities and rates. Biochimica et biophysica acta. 1830 (12), 5444-5455. https://doi.org/10.1016/j.bbagen.2013.06.018

Basset, C., Averseng, O., Ferron, P.J., Richaud, N., Hagege, A., Pible, O., Vidaud, C., 2013. Revision of the biodistribution of uranyl in serum: is fetuin-A the major protein target? Chemical research in toxicology. 26 (5), 645-653. https://doi.org/10.1021/tx400048u

Basset, C., Dedieu, A., Guérin, P., Quéméneur, E., Meyer, D., Vidaud, C., 2008. Specific capture of uranyl protein targets by metal affinity chromatography. Journal of Chromatography A. 1185 (2), 233-240. https://doi.org/10.1016/j.chroma.2008.01.081

Bensmihen, S., To, A., Lambert, G., Kroj, T., Giraudat, J., Parcy, F., 2004. Analysis of an activated ABI5 allele using a new selection method for transgenic Arabidopsis seeds. FEBS Letters. 561 (1-3), 127-131. https://doi.org/https://doi.org/10.1016/S0014-5793(04)00148-6

Berthet, S., Villiers, F., Alban, C., Serre, N.B.C., Martin-Laffon, J., Figuet, S., Boisson, A.M., Bligny, R., Kuntz, M., Finazzi, G., Ravanel, S., Bourguignon, J., 2018. Arabidopsis thaliana plants challenged with uranium reveal new insights into iron and phosphate homeostasis. New Phytologist. 217 (2), 657-670. https://doi.org/10.1111/nph.14865

Binstead, R.A., Zuberbühler, A.D., Jung, B., 2003. Specfit Global Analysis System Version 3.0.34. Spectrum Software Associates, Marlborough MA.

Boeri Erba, E., Signor, L., Oliva, M.F., Hans, F., Petosa, C., 2018. Characterizing Intact Macromolecular Complexes Using Native Mass Spectrometry. in: Marsh, J.A., ed, Protein Complex Assembly: Methods and Protocols, Springer New York, New York, NY, pp 133-151.

Bradford, M.M., 1976. A rapid and sensitive method for the quantitation of microgram quantities of protein utilizing the principle of protein-dye binding. Analytical biochemistry. 72, 248-254. https://doi.org/10.1006/abio.1976.9999

Bucher, G., Frelon, S., Simon, O., Lobinski, R., Mounicou, S., 2014. Development of non-denaturing off-gel isoelectric focusing for the separation of uranium–protein complexes in fish. Analytical and bioanalytical chemistry. 406 (14), 3517-3520. https://doi.org/10.1007/s00216-014-7768-x

Bucher, G., Mounicou, S., Simon, O., Floriani, M., Lobinski, R., Frelon, S., 2016. Insights into the nature of uranium target proteins within zebrafish gills after chronic and acute waterborne exposures. Environmental toxicology and chemistry. 35 (3), 736-741. https://doi.org/10.1002/etc.3249

Cheng, G., Yang, Z., Zhang, H., Zhang, J., Xu, J., 2020. Remorin interacting with PCaP1 impairs Turnip mosaic virus intercellular movement but is antagonised by VPg. New Phytologist. 225 (5), 2122-2139. https://doi.org/https://doi.org/10.1111/nph.16285

Clough, S.J., Bent, A.F., 1998. Floral dip: a simplified method for Agrobacterium -mediated transformation of Arabidopsis thaliana. The Plant Journal. 16 (6), 735-743. https://doi.org/https://doi.org/10.1046/j.1365-313x.1998.00343.x

Creff, G., Zurita, C., Jeanson, A., Carle, G., Vidaud, C., Den Auwer, C., 2019. What do we know about actinides-proteins interactions? Radiochimica Acta. 107 (9-11), 993-1009. https://doi.org/10.1515/ract-2019-3120

Cvetkovic, A., Menon, A.L., Thorgersen, M.P., Scott, J.W., Poole, F.L., 2nd, Jenney, F.E., Jr., Lancaster, W.A., Praissman, J.L., Shanmukh, S., Vaccaro, B.J., Trauger, S.A., Kalisiak, E., Apon, J.V., Siuzdak, G., Yannone, S.M., Tainer, J.A., Adams, M.W., 2010. Microbial metalloproteomes are largely uncharacterized. Nature. 466 (7307), 779-782. https://doi.org/10.1038/nature09265

Dedieu, A., Bérenguer, F., Basset, C., Prat, O., Quéméneur, E., Pible, O., Vidaud, C., 2009. Identification of uranyl binding proteins from human kidney-2 cell extracts by immobilized uranyl affinity chromatography and mass spectrometry. Journal of Chromatography A. 1216 (28), 5365-5376. https://doi.org/10.1016/j.chroma.2009.05.023

Doustaly, F., Combes, F., Fievet, J.B., Berthet, S., Hugouvieux, V., Bastien, O., Aranjuelo, I., Leonhardt, N., Rivasseau, C., Carriere, M., Vavasseur, A., Renou, J.P., Vandenbrouck,

Y., Bourguignon, J., 2014. Uranium perturbs signaling and iron uptake response in Arabidopsis thaliana roots. Metallomics : integrated biometal science. 6 (4), 809-821. https://doi.org/10.1039/c4mt00005f

Eb-Levadoux, Y., Frelon, S., Simon, O., Arnaudguilhem, C., Lobinski, R., Mounicou, S., 2017. In vivo identification of potential uranium protein targets in zebrafish ovaries after chronic waterborne exposure. Metallomics : integrated biometal science. 9 (5), 525-534. https://doi.org/10.1039/c6mt00291a

Ebbs, S.D., Brady, D.J., Kochian, L.V., 1998. Role of uranium speciation in the uptake and translocation of uranium by plants. Journal of Experimental Botany. 49 (324), 1183-1190. https://doi.org/10.1093/jxb/49.324.1183

Farrow, N.A., Muhandiram, R., Singer, A.U., Pascal, S.M., Kay, C.M., Gish, G., Shoelson, S.E., Pawson, T., Forman-Kay, J.D., Kay, L.E., 1994. Backbone Dynamics of a Free and a Phosphopeptide-Complexed Src Homology 2 Domain Studied by 15N NMR Relaxation. Biochemistry. 33 (19), 5984-6003. https://doi.org/10.1021/bi00185a040

Favier, A., Brutscher, B., 2011. Recovering lost magnetization: polarization enhancement in biomolecular NMR. Journal of Biomolecular NMR. 49 (1), 9-15. https://doi.org/10.1007/s10858-010-9461-5

Favier, A., Brutscher, B., 2019. NMRlib: user-friendly pulse sequence tools for Bruker NMR spectrometers. Journal of Biomolecular NMR. 73 (5), 199-211. https://doi.org/10.1007/s10858-019-00249-1

Frelon, S., Guipaud, O., Mounicou, S., Lobinski, R., Delissen, O., Paquet, F., 2009. In vivo screening of proteins likely to bind uranium in exposed rat kidney. Radiochimica Acta. 97 (7), 367-373. https://doi.org/10.1524/ract.2009.1619

Gallois, N., Alpha-Bazin, B., Bremond, N., Ortet, P., Barakat, M., Piette, L., Mohamad Ali, A., Lemaire, D., Legrand, P., Theodorakopoulos, N., Floriani, M., Fevrier, L., Den Auwer, C., Arnoux, P., Berthomieu, C., Armengaud, J., Chapon, V., 2021. Discovery and characterization of UipA, a uranium- and iron-binding PepSY protein involved in uranium tolerance by soil bacteria. The ISME journal. https://doi.org/10.1038/s41396-021-01113-7

Gampp, H., Maeder, M., Meyer, C.J., Zuberbühler, A.D., 1985. Calculation of equilibrium constants from multiwavelength spectroscopic data—II132, 95.: Specfit: two user-friendly programs in basic and standard fortran 77. Talanta. 32 (4), 257-264. https://doi.org/https://doi.org/10.1016/0039-9140(85)80077-1

Garai, A., Delangle, P., 2020. Recent advances in uranyl binding in proteins thanks to biomimetic peptides. Journal of Inorganic Biochemistry. 203, 110936. https://doi.org/10.1016/j.jinorgbio.2019.110936

Giovannoni, M., Marti, L., Ferrari, S., Tanaka-Takada, N., Maeshima, M., Ott, T., De Lorenzo, G., Mattei, B., 2021. The plasma membrane-associated Ca(2+) -binding protein, PCaP1, is required for oligogalacturonide and flagellin-induced priming and immunity. Plant, cell & environment. 44 (9), 3078-3093. https://doi.org/10.1111/pce.14118

Hartmann, E.M., Allain, F., Gaillard, J.-C., Pible, O., Armengaud, J., 2014. Taking the Shortcut for High-Throughput Shotgun Proteomic Analysis of Bacteria. in: Vergunst, A.C., O'Callaghan, D., eds. Host-Bacteria Interactions: Methods and Protocols, Springer New York, New York, NY, pp 275-285.

Hetherington, A.M., Woodward, F.I., 2003. The role of stomata in sensing and driving environmental change. Nature. 424 (6951), 901-908. https://doi.org/10.1038/nature01843

Hoarau, M., Koebke, K.J., Chen, Z., Marsh, E.N.G., 2019. Probing Metal Ion Discrimination in a Protein Designed to Bind Uranyl Cation With Femtomolar Affinity. Frontiers in molecular biosciences. 6, 73. https://doi.org/10.3389/fmolb.2019.00073

Huynh, T.N., Bourgeois, D., Basset, C., Vidaud, C., Hagege, A., 2015. Assessment of CE-ICP/MS hyphenation for the study of uranyl/protein interactions. Electrophoresis. 36 (11-12), 1374-1382. https://doi.org/10.1002/elps.201400471

Huynh, T.S., Vidaud, C., Hagege, A., 2016. Investigation of uranium interactions with calcium phosphate-binding proteins using ICP/MS and CE-ICP/MS. Metallomics : integrated biometal science. 8 (11), 1185-1192. https://doi.org/10.1039/c6mt00147e

Ide, Y., Nagasaki, N., Tomioka, R., Suito, M., Kamiya, T., Maeshima, M., 2007. Molecular properties of a novel, hydrophilic cation-binding protein associated with the plasma membrane. Journal of Experimental Botany. 58 (5), 1173-1183. https://doi.org/10.1093/jxb/erl284

Jiang, J., Sarsfield, M.J., Renshaw, J.C., Livens, F.R., Collison, D., Charnock, J.M., Helliwell, M., Eccles, H., 2002. Synthesis and Characterization of Uranyl Compounds with Iminodiacetate and Oxydiacetate Displaying Variable Denticity. Inorganic chemistry. 41 (10), 2799-2806. https://doi.org/10.1021/ic020121v

Johnson, C.S., 1999. Diffusion ordered nuclear magnetic resonance spectroscopy: principles and applications. Progress in Nuclear Magnetic Resonance Spectroscopy. 34 (3), 203-256. https://doi.org/https://doi.org/10.1016/S0079-6565(99)00003-5

Jumper, J., Evans, R., Pritzel, A., Green, T., Figurnov, M., Ronneberger, O., Tunyasuvunakool, K., Bates, R., Žídek, A., Potapenko, A., Bridgland, A., Meyer, C., Kohl, S.A.A., Ballard, A.J., Cowie, A., Romera-Paredes, B., Nikolov, S., Jain, R., Adler, J., Back, T., Petersen, S., Reiman, D., Clancy, E., Zielinski, M., Steinegger, M., Pacholska, M., Berghammer, T., Bodenstein, S., Silver, D., Vinyals, O., Senior, A.W., Kavukcuoglu, K., Kohli, P., Hassabis, D., 2021. Highly accurate protein structure prediction with AlphaFold. Nature. 596 (7873), 583-589. https://doi.org/10.1038/s41586-021-03819-2

Kato, M., Nagasaki-Takeuchi, N., Ide, Y., Tomioka, R., Maeshima, M., 2010. PCaPs, possible regulators of PtdInsP signals on plasma membrane. Plant Signaling & Behavior. 5 (7), 848-850. https://doi.org/10.4161/psb.5.7.11825

Konietschke, F., Placzek, M., Schaarschmidt, F., Hothorn, L.A., 2015. nparcomp : An R Software Package for Nonparametric Multiple Comparisons and Simultaneous Confidence Intervals. Journal of Statistical Software. 64 (9), 1-17. https://doi.org/10.18637/jss.v064.i09

Lai, J.L., Liu, Z.W., Luo, X.G., 2020. A metabolomic, transcriptomic profiling, and mineral nutrient metabolism study of the phytotoxicity mechanism of uranium. Journal of hazardous materials. 386, 121437. https://doi.org/10.1016/j.jhazmat.2019.121437

Laporte, F.A., Lebrun, C., Vidaud, C., Delangle, P., 2019. Phosphate-Rich Biomimetic Peptides Shed Light on High-Affinity Hyperphosphorylated Uranyl Binding Sites in Phosphoproteins. Chemistry. 25 (36), 8570-8578. https://doi.org/10.1002/chem.201900646

Laurette, J., Larue, C., Mariet, C., Brisset, F., Khodja, H., Bourguignon, J., Carrière, M., 2012. Influence of uranium speciation on its accumulation and translocation in three plant species: Oilseed rape, sunflower and wheat. Environmental and Experimental Botany. 77, 96-107. https://doi.org/10.1016/j.envexpbot.2011.11.007

Le Clainche, L., Vita, C., 2006. Selective binding of uranyl cation by a novel calmodulin peptide. Environmental Chemistry Letters. 4 (1), 45-49. https://doi.org/10.1007/s10311-005-0033-y

Lebrun, C., Starck, M., Gathu, V., Chenavier, Y., Delangle, P., 2014. Engineering short peptide sequences for uranyl binding. Chemistry. 20 (50), 16566-16573. https://doi.org/10.1002/chem.201404546

Li, J.J., Wang, X.L., Qin, T., Zhang, Y., Liu, X.M., Sun, J.B., Zhou, Y., Zhu, L., Zhang, Z.D., Yuan, M., Mao, T.L., 2011. MDP25, A Novel Calcium Regulatory Protein, Mediates Hypocotyl Cell Elongation by Destabilizing Cortical Microtubules in Arabidopsis. Plant Cell. 23 (12), 4411-4427. https://doi.org/10.1105/tpc.111.092684

Lin, Y.W., 2020. Uranyl Binding to Proteins and Structural-Functional Impacts. Biomolecules. 10 (3)https://doi.org/10.3390/biom10030457

Lin, Y.W., Nie, C.M., Liao, L.F., 2011. Insights into Uranyl Ion Binding to Ubiquitin from Molecular Modeling and Dynamics Simulations. Chem Lett. 40 (12), 1330-1331. https://doi.org/10.1246/cl.2011.1330

Marty, M.T., Baldwin, A.J., Marklund, E.G., Hochberg, G.K.A., Benesch, J.L.P., Robinson, C.V., 2015. Bayesian Deconvolution of Mass and Ion Mobility Spectra: From Binary Interactions to Polydisperse Ensembles. Analytical Chemistry. 87 (8), 4370-4376. https://doi.org/10.1021/acs.analchem.5b00140

Mattei, B., Spinelli, F., Pontiggia, D., De Lorenzo, G., 2016. Comprehensive Analysis of the Membrane Phosphoproteome Regulated by Oligogalacturonides in Arabidopsis thaliana. Frontiers in plant science. 7, 1107. https://doi.org/10.3389/fpls.2016.01107

Mergner, J., Frejno, M., List, M., Papacek, M., Chen, X., Chaudhary, A., Samaras, P., Richter, S., Shikata, H., Messerer, M., Lang, D., Altmann, S., Cyprys, P., Zolg, D.P., Mathieson, T., Bantscheff, M., Hazarika, R.R., Schmidt, T., Dawid, C., Dunkel, A., Hofmann, T., Sprunck, S., Falter-Braun, P., Johannes, F., Mayer, K.F.X., Jürgens, G., Wilhelm, M., Baumbach, J., Grill, E., Schneitz, K., Schwechheimer, C., Kuster, B., 2020. Mass-spectrometry-based draft of the Arabidopsis proteome. Nature. 579 (7799), 409-414. https://doi.org/10.1038/s41586-020-2094-2

Michon, J., Frelon, S., Garnier, C., Coppin, F., 2010. Determinations of uranium(VI) binding properties with some metalloproteins (transferrin, albumin, metallothionein and ferritin) by fluorescence quenching. Journal of fluorescence. 20 (2), 581-590. https://doi.org/10.1007/s10895-009-0587-3

Misson, J., Henner, P., Morello, M., Floriani, M., Wu, T.-D., Guerquin-Kern, J.-L., Février, L., 2009. Use of phosphate to avoid uranium toxicity in Arabidopsis thaliana leads to alterations of morphological and physiological responses regulated by phosphate availability. Environmental and Experimental Botany. 67 (2), 353-362. https://doi.org/10.1016/j.envexpbot.2009.09.001

Morgner, N., Robinson, C.V., 2012. Massign: An Assignment Strategy for Maximizing Information from the Mass Spectra of Heterogeneous Protein Assemblies. Analytical Chemistry. 84 (6), 2939-2948. https://doi.org/10.1021/ac300056a

Nagasaki-Takeuchi, N., Miyano, M., Maeshima, M., 2008. A plasma membrane-associated protein of Arabidopsis thaliana AtPCaP1 binds copper ions and changes its higher order structure. Journal of biochemistry. 144 (4), 487-497. https://doi.org/10.1093/jb/mvn092

Nagasaki, N., Tomioka, R., Maeshima, M., 2008. A hydrophilic cation-binding protein of Arabidopsis thaliana, AtPCaP1, is localized to plasma membrane via N-myristoylation and interacts with calmodulin and the phosphatidylinositol phosphates PtdIns(3,4,5)P(3) and PtdIns(3,5)P(2). FEBS J. 275 (9), 2267-2282. https://doi.org/10.1111/j.1742-4658.2008.06379.x

Nagata, C., Miwa, C., Tanaka, N., Kato, M., Suito, M., Tsuchihira, A., Sato, Y., Segami, S., Maeshima, M., 2016. A novel-type phosphatidylinositol phosphate-interactive, Ca-binding protein PCaP1 in Arabidopsis thaliana: stable association with plasma membrane and partial involvement in stomata closure. J Plant Res. 129 (3), 539-550. https://doi.org/10.1007/s10265-016-0787-2

Pardoux, R., Sauge-Merle, S., Lemaire, D., Delangle, P., Guilloreau, L., Adriano, J.-M., Berthomieu, C., 2012. Modulating Uranium Binding Affinity in Engineered Calmodulin EF-Hand Peptides: Effect of Phosphorylation. PloS one. 7 (8), e41922-e41922. https://doi.org/10.1371/journal.pone.0041922

Pearson, R.G., 1963. Hard and Soft Acids and Bases. Journal of the American Chemical Society. 85 (22), 3533-3539. https://doi.org/10.1021/ja00905a001

Perez-Riverol, Y., Csordas, A., Bai, J., Bernal-Llinares, M., Hewapathirana, S., Kundu, D.J., Inuganti, A., Griss, J., Mayer, G., Eisenacher, M., Pérez, E., Uszkoreit, J., Pfeuffer, J., Sachsenberg, T., Yılmaz, Ş., Tiwary, S., Cox, J., Audain, E., Walzer, M., Jarnuczak, A.F., Ternent, T., Brazma, A., Vizcaíno, J.A., 2019. The PRIDE database and related tools and resources in 2019: improving support for quantification data. Nucleic Acids Research. 47 (D1), D442-D450. https://doi.org/10.1093/nar/gky1106

Puglisi, R., Boeri Erba, E., Pastore, A., 2020. A Guide to Native Mass Spectrometry to determine complex interactomes of molecular machines. The FEBS Journal. 287 (12), 2428-2439. https://doi.org/https://doi.org/10.1111/febs.15281

Qi, L., Basset, C., Averseng, O., Quemeneur, E., Hagege, A., Vidaud, C., 2014. Characterization of UO2(2+) binding to osteopontin, a highly phosphorylated protein: insights into potential mechanisms of uranyl accumulation in bones. Metallomics : integrated biometal science. 6 (1), 166-176. https://doi.org/10.1039/c3mt00269a

Qin, T., Liu, X.M., Li, J.J., Sun, J.B., Song, L.N., Mao, T.L., 2014. Arabidopsis Microtubule-Destabilizing Protein 25 Functions in Pollen Tube Growth by Severing Actin Filaments. Plant Cell. 26 (1), 325-339. https://doi.org/10.1105/tpc.113.119768

Rayapuram, N., Bonhomme, L., Bigeard, J., Haddadou, K., Przybylski, C., Hirt, H., Pflieger, D., 2014. Identification of novel PAMP-triggered phosphorylation and dephosphorylation events in Arabidopsis thaliana by quantitative phosphoproteomic analysis. Journal of proteome research. 13 (4), 2137-2151. https://doi.org/10.1021/pr401268v

Reiland, S., Messerli, G., Baerenfaller, K., Gerrits, B., Endler, A., Grossmann, J., Gruissem, W., Baginsky, S., 2009. Large-scale Arabidopsis phosphoproteome profiling reveals novel chloroplast kinase substrates and phosphorylation networks. Plant physiology. 150 (2), 889-903. https://doi.org/10.1104/pp.109.138677

Roeder, A.H.K., Otegui, M.S., Dixit, R., Anderson, C.T., Faulkner, C., Zhang, Y., Harrison, M.J., Kirchhelle, C., Goshima, G., Coate, J.E., Doyle, J.J., Hamant, O., Sugimoto, K., Dolan, L., Meyer, H., Ehrhardt, D.W., Boudaoud, A., Messina, C., 2022. Fifteen compelling open questions in plant cell biology. Plant Cell. 34 (1), 72-102. https://doi.org/10.1093/plcell/koab225

RStudio Team (2015) RStudio: Integrated Development Environment for R. RStudio, PBC., Boston, MA

Saenen, E., Horemans, N., Vanhoudt, N., Vandenhove, H., Biermans, G., Van Hees, M., Wannijn, J., Vangronsveld, J., Cuypers, A., 2014. The pH strongly influences the uranium-induced effects on the photosynthetic apparatus of Arabidopsis thaliana plants. Plant Physiology and Biochemistry. 82, 254-261. https://doi.org/10.1016/j.plaphy.2014.06.012

Saenen, E., Horemans, N., Vanhoudt, N., Vandenhove, H., Biermans, G., van Hees, M., Wannijn, J., Vangronsveld, J., Cuypers, A., 2015. Oxidative stress responses induced by uranium exposure at low pH in leaves of Arabidopsis thaliana plants. Journal of environmental radioactivity. 150, 36-43. https://doi.org/10.1016/j.jenvrad.2015.07.021

Safi, S., Creff, G., Jeanson, A., Qi, L., Basset, C., Roques, J., Solari, P.L., Simoni, E., Vidaud, C., Den Auwer, C., 2013. Osteopontin: a uranium phosphorylated binding-site characterization. Chemistry. 19 (34), 11261-11269. https://doi.org/10.1002/chem.201300989

Sarthou, M.C.M., Devime, F., Baggio, C., Figuet, S., Alban, C., Bourguignon, J., Ravanel, S., 2022. Calcium-permeable cation channels are involved in uranium uptake in Arabidopsis thaliana. Journal of hazardous materials. 424, 127436. https://doi.org/https://doi.org/10.1016/j.jhazmat.2021.127436

Sarthou, M.C.M., Revel, B.H., Villiers, F., Alban, C., Bonnot, T., Gigarel, O., Boisson, A.-M., Ravanel, S., Bourguignon, J., 2020. Development of a metalloproteomic approach to analyse the response of Arabidopsis cells to uranium stress. Metallomics : integrated biometal science. 12 (8), 1302-1313. https://doi.org/10.1039/d0mt00092b

Sauge-Merle, S., Brulfert, F., Pardoux, R., Solari, P.L., Lemaire, D., Safi, S., Guilbaud, P., Simoni, E., Merroun, M.L., Berthomieu, C., 2017. Structural Analysis of Uranyl Complexation by the EF-Hand Motif of Calmodulin: Effect of Phosphorylation. Chemistry. 23 (61), 15505-15517. https://doi.org/10.1002/chem.201703484

Schanda, P., Forge, V., Brutscher, B., 2006. HET-SOFAST NMR for fast detection of structural compactness and heterogeneity along polypeptide chains. Magnetic Resonance in Chemistry. 44 (S1), S177-S184. https://doi.org/https://doi.org/10.1002/mrc.1825

Serre, N.B.C., Alban, C., Bourguignon, J., Ravanel, S., 2019. Uncovering the physiological and cellular effects of uranium on the root system of Arabidopsis thaliana. Environmental and Experimental Botany. 157, 121-130. https://doi.org/10.1016/j.envexpbot.2018.10.004

Solyom, Z., Schwarten, M., Geist, L., Konrat, R., Willbold, D., Brutscher, B., 2013. BEST-TROSY experiments for time-efficient sequential resonance assignment of large disordered proteins. Journal of Biomolecular NMR. 55 (4), 311-321. https://doi.org/10.1007/s10858-013-9715-0

Starck, M., Laporte, F.A., Oros, S., Sisommay, N., Gathu, V., Solari, P.L., Creff, G., Roques, J., Den Auwer, C., Lebrun, C., Delangle, P., 2017. Cyclic Phosphopeptides to Rationalize the Role of Phosphoamino Acids in Uranyl Binding to Biological Targets. Chemistry. 23 (22), 5281-5290. https://doi.org/10.1002/chem.201605481

Starck, M., Sisommay, N., Laporte, F.A., Oros, S., Lebrun, C., Delangle, P., 2015. Preorganized Peptide Scaffolds as Mimics of Phosphorylated Proteins Binding Sites with a High Affinity for Uranyl. Inorganic chemistry. 54 (23), 11557-11562. https://doi.org/10.1021/acs.inorgchem.5b02249

Sun, M.-H., Liu, S.-Q., Du, K.-J., Nie, C.-M., Lin, Y.-W., 2014. A spectroscopic study of uranyl-cytochrome b5/cytochrome c interactions. Spectrochimica Acta Part A: Molecular and Biomolecular Spectroscopy. 118, 130-137. https://doi.org/10.1016/j.saa.2013.08.112

Tanaka-Takada, N., Kobayashi, A., Takahashi, H., Kamiya, T., Kinoshita, T., Maeshima, M., 2019. Plasma Membrane-Associated Ca2+-Binding Protein PCaP1 is Involved in Root Hydrotropism of Arabidopsis thaliana. Plant and Cell Physiology. 60 (6), 1331-1341. https://doi.org/10.1093/pcp/pcz042

Tewari, R., Horemans, N., Nauts, R., Wannijn, J., Van Hees, M., Vandenhove, H., 2015. Uranium exposure induces nitric oxide and hydrogen peroxide generation in Arabidopsis thaliana. Environmental and Experimental Botany. 120, 55-64. https://doi.org/10.1016/j.envexpbot.2015.08.004

Tsuji, J., Nydza, R., Wolcott, E., Mannor, E., Moran, B., Hesson, G., Arvidson, T., Howe, K., Hayes, R., Ramirez, M., Way, M., 2010. The Frequencies of Amino Acids Encoded by Genomes that Utilize Standard and Nonstandard Genetic Codes. BIOS. 81 (1), 22-31, 10.

Van Horn, J., Huang, H., 2006. Uranium(VI) bio-coordination chemistry from biochemical, solution and protein structural data. Coordin Chem Rev. 250 (7-8), 765-775. https://doi.org/10.1016/j.ccr.2005.09.010

van Wijk, K.J., Friso, G., Walther, D., Schulze, W.X., 2014. Meta-Analysis of Arabidopsis thaliana Phospho-Proteomics Data Reveals Compartmentalization of Phosphorylation Motifs The Plant Cell. 26 (6), 2367-2389. https://doi.org/10.1105/tpc.114.125815

Vanhoudt, N., Horemans, N., Biermans, G., Saenen, E., Wannijn, J., Nauts, R., Van Hees, M., Vandenhove, H., 2014. Uranium affects photosynthetic parameters in Arabidopsis thaliana. Environmental and Experimental Botany. 97, 22-29. https://doi.org/10.1016/j.envexpbot.2013.09.009

Vanhoudt, N., Vandenhove, H., Horemans, N., Bello, D.M., Van Hees, M., Wannijn, J., Carleer, R., Vangronsveld, J., Cuypers, A., 2011. Uranium Induced Effects on Development and Mineral Nutrition of Arabidopsis Thaliana. J Plant Nutr. 34 (13), 1940-1956. https://doi.org/10.1080/01904167.2011.610482

Vanhoudt, N., Vandenhove, H., Smeets, K., Remans, T., Van Hees, M., Wannijn, J., Vangronsveld, J., Cuypers, A., 2008. Effects of uranium and phosphate concentrations on oxidative stress related responses induced in Arabidopsis thaliana. Plant Physiology and Biochemistry. 46 (11), 987-996. https://doi.org/10.1016/j.plaphy.2008.06.003

Vidaud, C., Dedieu, A., Basset, C., Plantevin, S., Dany, I., Pible, O., Quemeneur, E., 2005. Screening of human serum proteins for uranium binding. Chemical research in toxicology. 18 (6), 946-953. https://doi.org/10.1021/tx050038v

Vidaud, C., Gourion-Arsiquaud, S., Rollin-Genetet, F., Torne-Celer, C., Plantevin, S., Pible, O., Berthomieu, C., Quemeneur, E., 2007. Structural consequences of binding of UO2(2+) to apotransferrin: can this protein account for entry of uranium into human cells? Biochemistry. 46 (8), 2215-2226. https://doi.org/10.1021/bi061945h

Vidaud, C., Robert, M., Paredes, E., Ortega, R., Avazeri, E., Jing, L., Guigonis, J.M., Bresson, C., Malard, V., 2019. Deciphering the uranium target proteins in human dopaminergic

SH-SY5Y cells. Archives of toxicology. 93 (8), 2141-2154. https://doi.org/10.1007/s00204-019-02497-4

Vijayapalani, P., Maeshima, M., Nagasaki-Takekuchi, N., Miller, W.A., 2012. Interaction of the Trans-Frame Potyvirus Protein P3N-PIPO with Host Protein PCaP1 Facilitates Potyvirus Movement. PLOS Pathogens. 8 (4), e1002639. https://doi.org/10.1371/journal.ppat.1002639

Wan, D., Liao, L.F., Zhao, M.M., Wu, M.L., Wu, Y.M., Lin, Y.W., 2012. Interactions of uranyl ion with cytochrome b(5) and its His39Ser variant as revealed by molecular simulation in combination with experimental methods. Journal of molecular modeling. 18 (3), 1009-1013. https://doi.org/10.1007/s00894-011-1097-1

Wegner, S.V., Boyaci, H., Chen, H., Jensen, M.P., He, C., 2009. Engineering a uranyl-specific binding protein from NikR. Angew Chem Int Ed Engl. 48 (13), 2339-2341. https://doi.org/10.1002/anie.200805262

Xu, M., Frelon, S., Simon, O., Lobinski, R., Mounicou, S., 2014. Non-denaturating isoelectric focusing gel electrophoresis for uranium-protein complexes quantitative analysis with LA-ICP MS. Analytical and bioanalytical chemistry. 406 (4), 1063-1072. https://doi.org/10.1007/s00216-013-7033-8

Zhou, L., Bosscher, M., Zhang, C., Ozcubukcu, S., Zhang, L., Zhang, W., Li, C.J., Liu, J., Jensen, M.P., Lai, L., He, C., 2014. A protein engineered to bind uranyl selectively and with femtomolar affinity. Nature chemistry. 6 (3), 236-241. https://doi.org/10.1038/nchem.1856

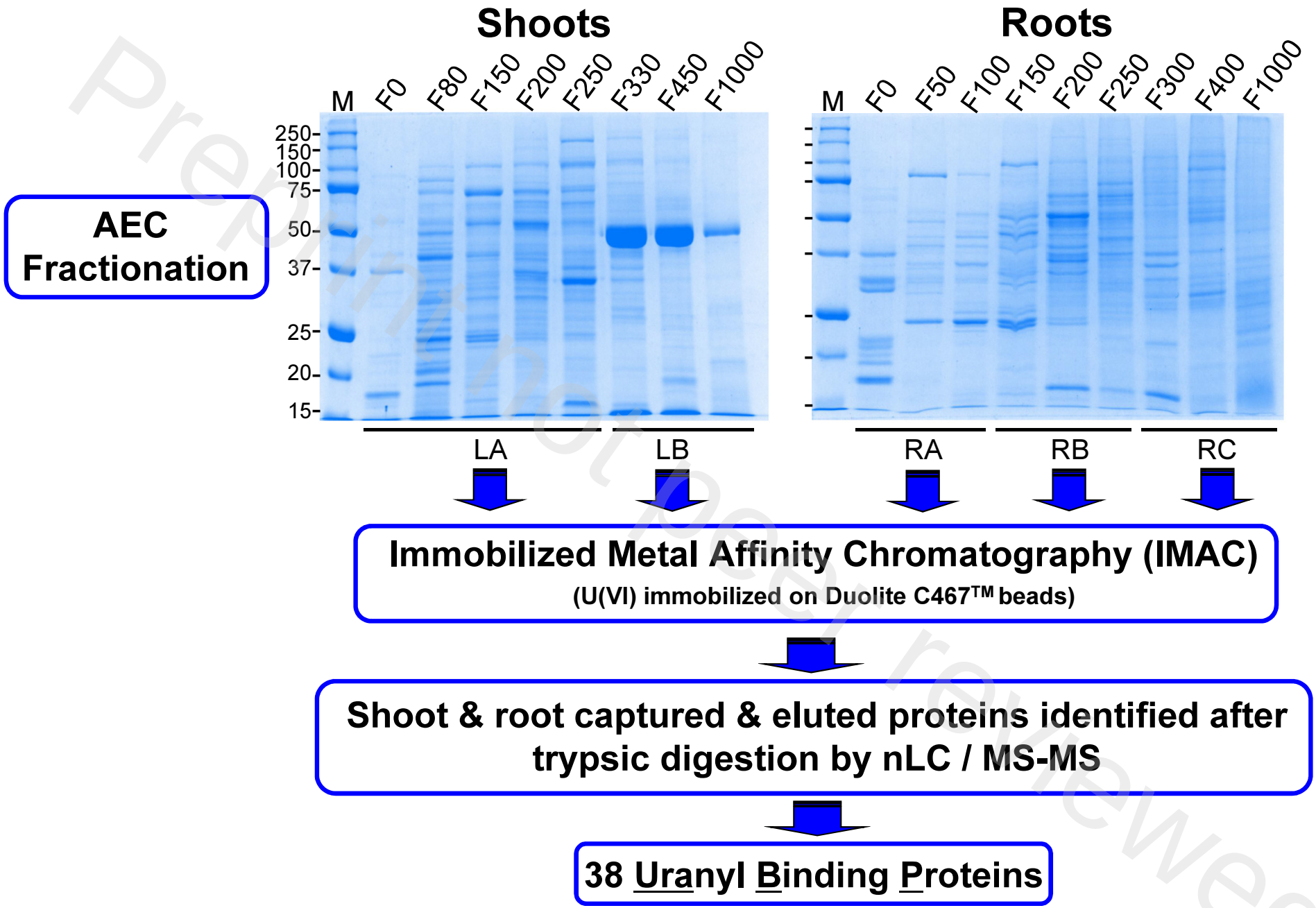

Figure 1: Strategy for the isolation and identification of uranyl-binding proteins from *Arabidopsis thaliana*.

Figure 1

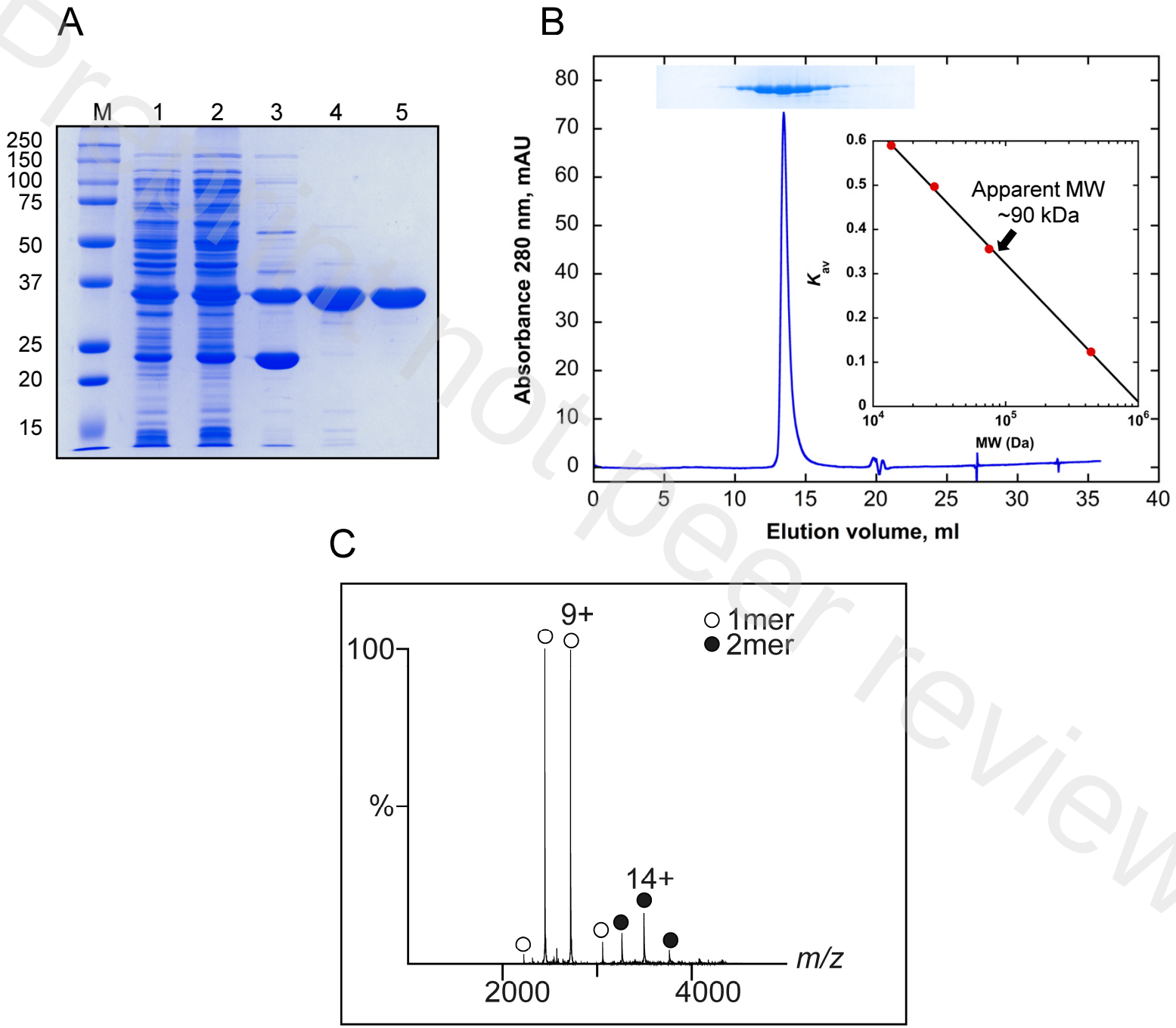

Figure 2 (legend on the next page)

Figure 2: Purification of recombinant PCaP1 and determination of its oligomerization state. A- Documentation of PCaP1 purification. Polypeptides were separated by SDS-PAGE 12% and stained with Coomassie Brilliant Blue R250. Lane 1: soluble proteins (25 µg) from *E. coli* Rosetta cells harboring pET28-PCaP1 construct grown in the presence of IPTG; Lane 2: ammonium sulfate 50% of saturation precipitating fraction (25 µg); Lane 3: BioGel HTP hydroxyapatite column pool (15 µg); Lane 4: EMD-DEAE column pool (10 µg); Superdex 75 column pool (8 µg); M, molecular mass markers. B- Apparent molecular mass estimation of native recombinant PCaP1 by gel filtration. Purified protein (150 µg) was resolved by size exclusion chromatography (SEC) onto a Superdex 200 Increase 10/300 GL column. Eluted fractions were analyzed by SDS-PAGE. Standard proteins for column calibration (inset) were ferritin (440 kDa), covalbumin (75 kDa), carbonic anhydrase (29 kDa), and ribonuclease A (13.7 kDa). K_{av} = (Ve-Vo)/(Vt-Vo); Ve, elution volume; Vo, void volume; Vt, total volume. C- Native mass spectrum of recombinant PCaP1. 1mer (monomer) = 24453 Da; 2mer (dimer) = 48906 Da.

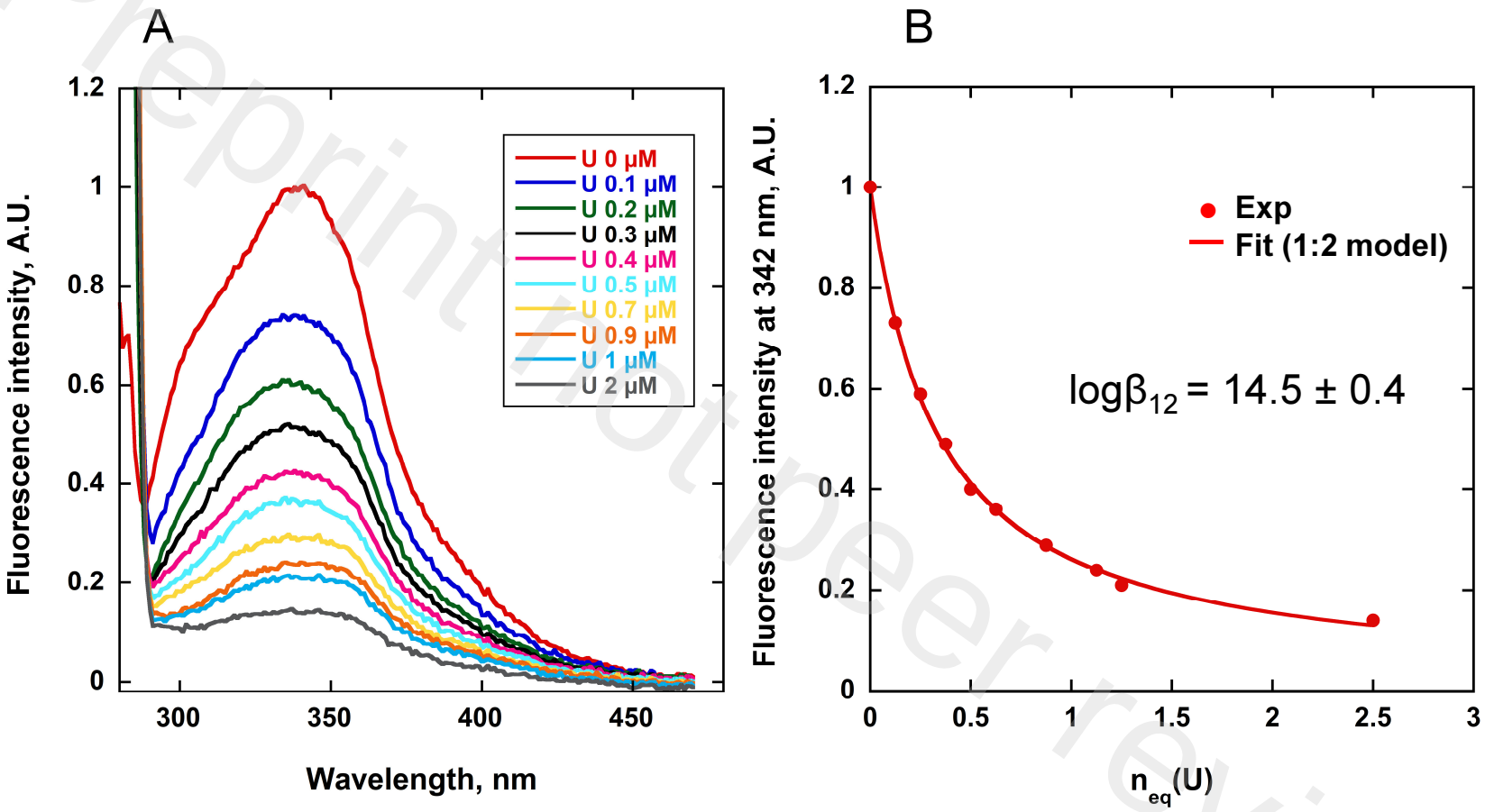

Figure 3: Fluorescence emission spectrum analysis of uranyl binding to PCaP1 at pH 6. A- Fluorescence titration of recombinant PCaP1 (0.8 µM) with UO_2^{2+} (0 to 2.5 equivalents) at pH 6 in MES buffer 10 mM, NaCl 100 mM, in the presence of IDA 10 µM, with excitation at 277 nm. B- Variation of the intensity at the peak maximum (342 nm) upon UO_2^{2+} addition. Circles represent experimental (Exp) values and the solid line the best fit with the program SPECFIT, taking into consideration the known conditional stability constants of the uranyl complexes with IDA. $n_{eq}(U)$, number of U(VI) equivalents ([U(VI)]/[PCaP1]).

Figure 3

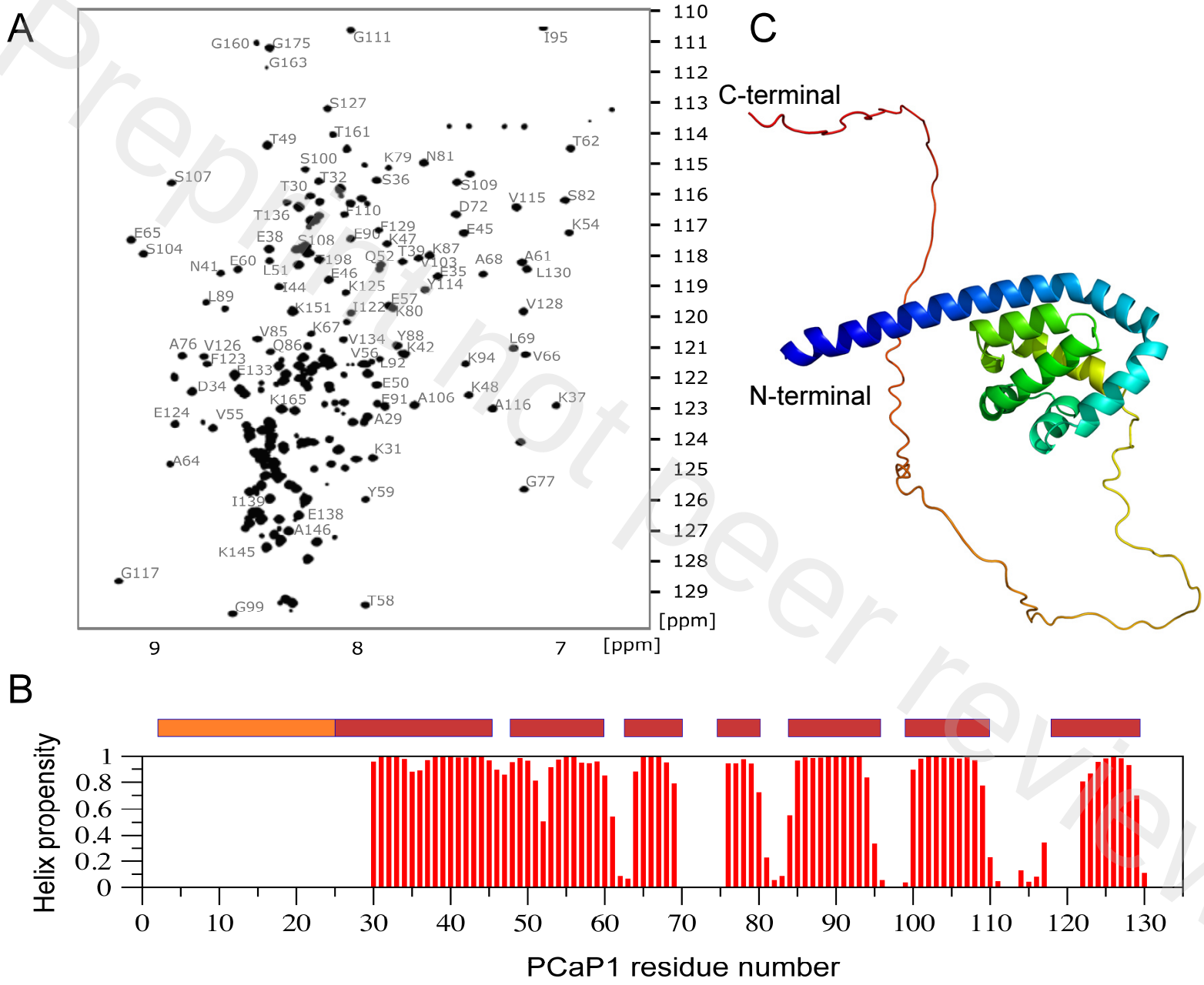

Figure 4 (legend on the next page)

Figure 4: NMR assignment and structural features of PCaP1. A- Amide ^{1}H-^{15}N correlation spectrum of free PCaP1. Resolved cross peaks are annotated by their residue type (one letter amino acid code) and residue number. Sample: PCaP1 300 µM in Tris-HCl 10 mM pH 7.5, NaN_3 0.03%. B- Helical propensity along the PCaP1 backbone (only the structured part is shown) computed from the measured ^{13}C chemical shifts using the TALOS-N server (https://spin.niddk.nih.gov/bax/software/TALOS-N/). The helical elements derived from this plot (red bars) are in agreement with the structure predicted by Alpha Fold v2.0 (https://alphafold.ebi.ac.uk/) shown in (C). Model confidence (pLDDT score) for the structured domain was >90 (highly confident).The image was produced using PyMOL (DeLano Scientific, San Carlos, CA, USA) as a ribbon model colored in the “chainbows” mode.

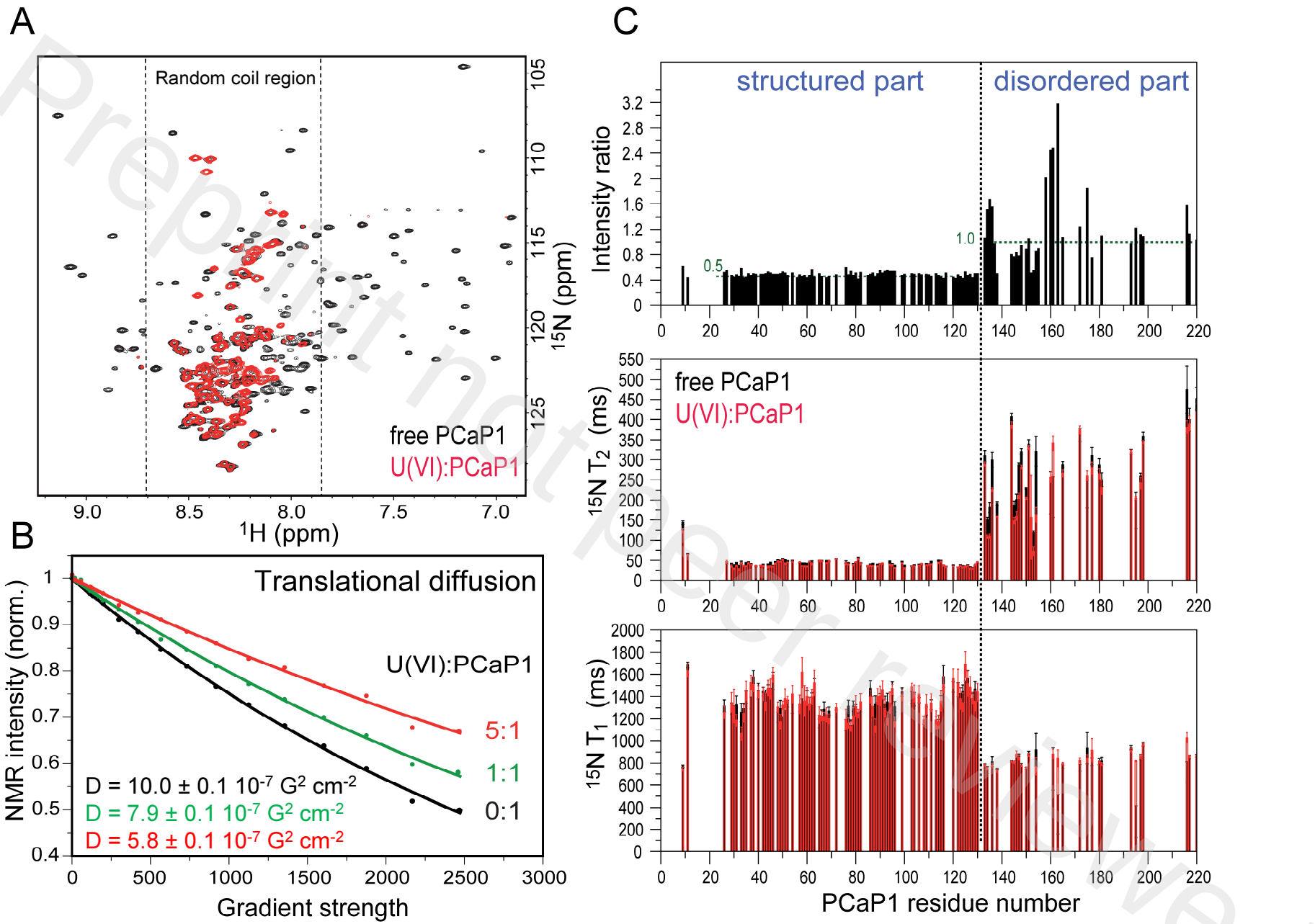

Figure 5 (legend on the next page)

Figure 5: NMR characterization of PCaP1-U(VI) interaction. A- Overlay of 2D ^{1}H-^{15}N correlation spectra of free ^{15}N-^{13}C labelled PCaP1 (100 µM) alone (black) or in complex (100 µM) with U(VI) (500 µM) (red) in Tris-HCl 10 mM pH 7.5. Only correlation peaks in the random coil ^{1}H spectral region (indicated by dashed lines) remain visible upon U(VI) binding. B- Diffusion ordered spectroscopy (DOSY) measurements of PCaP1 in the absence or in the presence of 1 or 5 U(VI) equivalents. The observed NMR signal intensity (integrated over the 1D ^{1}H spectrum) is plotted as a function of the applied gradient strength. Fitting of decay curves yields the translational diffusion constant. Translational diffusion of PCaP1 decreases U(VI) with increasing amounts of uranyl, indicating the formation of larger particles. C- ^{15}N spin relaxation rate constants (T_1 and T_2) measured for free PcaP1 (black) and PCaP1 in the presence of an equal amount of U(VI) (red). In addition, the intensity ratios of ^{1}H-^{15}N correlation peaks detected in the absence and presence of an equal amount of U(VI) are plotted (top panel).

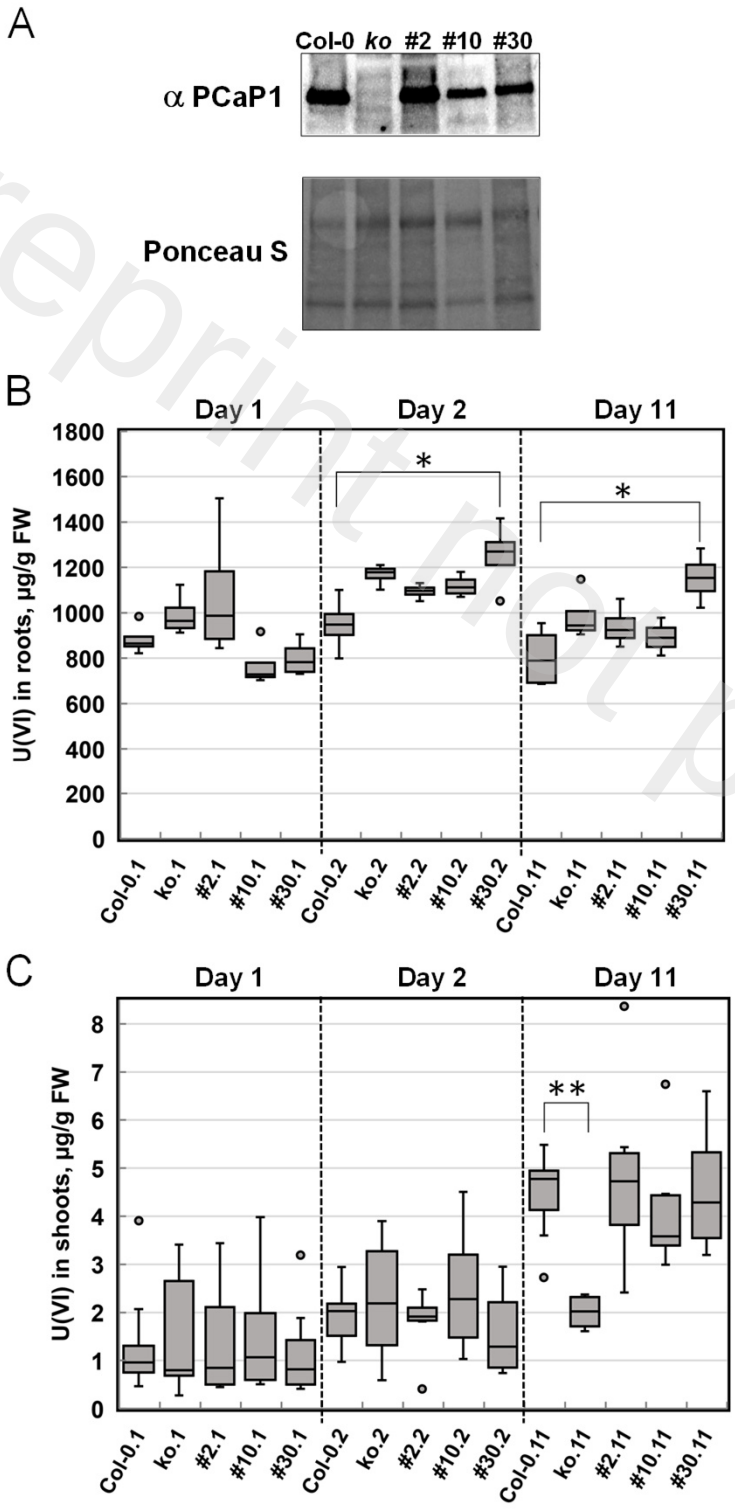

Figure 6

Figure 6: Uranium content in wild type, *pcap1*-null mutant and transgenic lines expressing PCaP1. Wild type (Col-0), *pcap1*-null mutant (*ko*) and transgenic lines expressing PCaP1 under the control of a 35S promoter (#2; #10 and #30 lines) were grown hydroponically for 5 weeks in Gre medium, and then challenged with 20 µM uranyl nitrate for 1, 2 and 11 days in Gre medium with no phosphate. A- Western blot analysis of total shoot proteins with a PCaP1 antibody. B- Accumulation of U in roots. C- Accumulation of U in shoots. Samples were dehydrated, digested with HNO_3, and ^{238}U was measured by ICP-MS. Data distribution is displayed in Tukey's boxplots with the median as the solid line inside the box, and the first and third quartiles as the bottom and top lines of the box, respectively. Outliers are shown as individual dots. Each distribution in boxplots represents n = 4 samples for roots and n = 4-8 samples for shoots. Statistical significance determined using non-parametric comparisons with Tukey's test is shown: *, $p < 0.05$; **, $p < 0.01$.

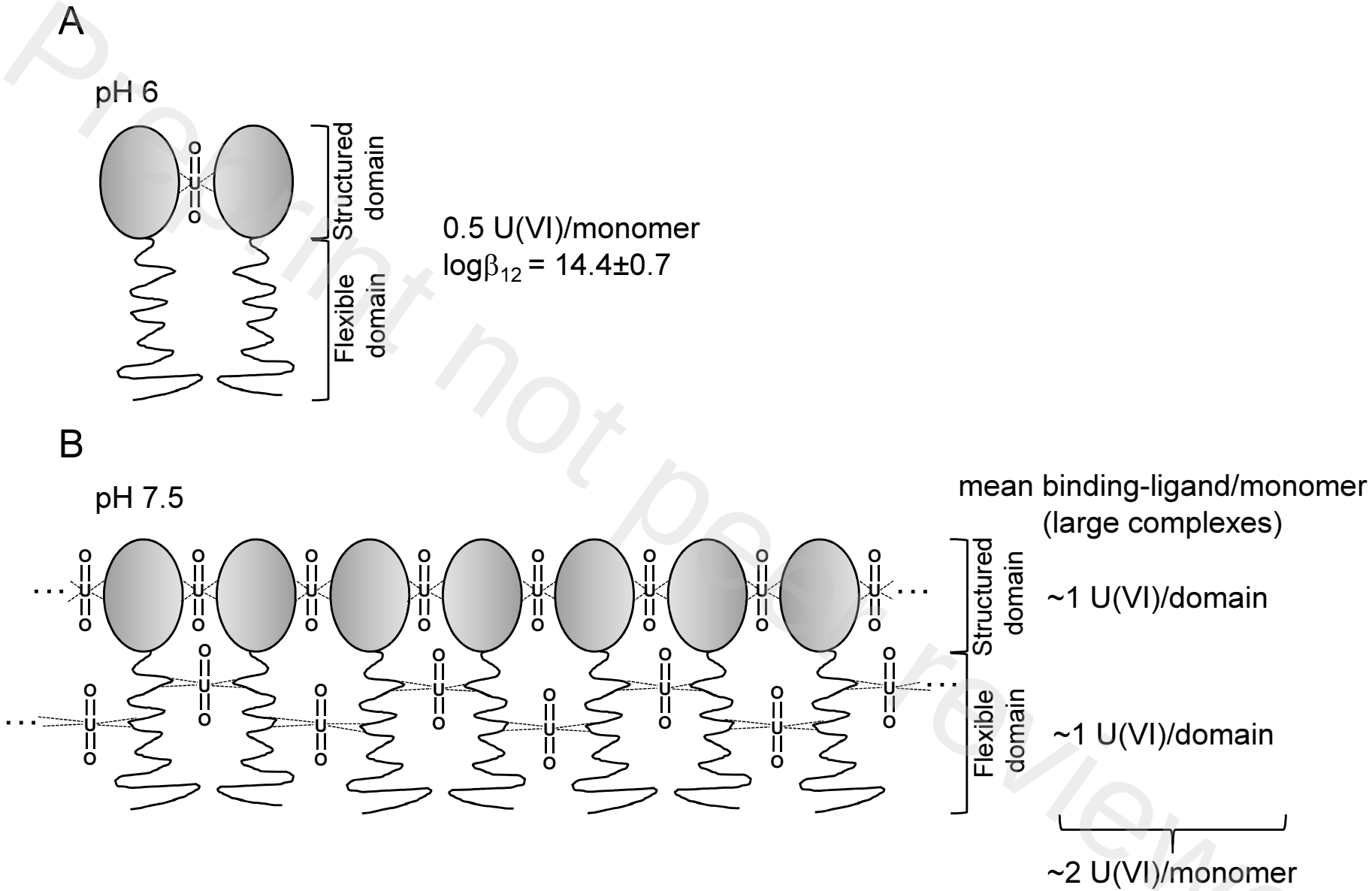

Figure 7: Models for *in vitro* U(VI)-PCaP1 complexes formation at pH 6 and pH 7.5.

Figure 7